

# Integrated Coastal-River-Urban Total Water Level Forecast System for Tidal Rivers: Calibration, Validation, and Operational Evaluation

Arslaan Khalid<sup>1</sup>, Celso M Ferreira<sup>1</sup>, and Jason Elliott<sup>2</sup>

<sup>1</sup>George Mason University

<sup>2</sup>National Weather Service

November 23, 2022

## Abstract

Existing real-time coastal flooding guidance systems in the US tend to underestimate total water level (TWL) predictions in upstream tidal areas of the Chesapeake Bay rivers, impacting flood forecasts for highly vulnerable areas, such as the National Capital Region. These under-predictions are mostly due to missing physical processes, lack of integration between hydrological and hydrodynamic models, and an oversimplification of the model setups used to predict TWL. In this study, an integrated TWL forecast system was introduced, where a high-resolution two-dimensional coastal storm surge model (ADCIRC) was implemented to simulate the combined influence of various flood drivers (storm tide, river flows, urban runoff, and local wind forcing) in the Potomac River. In this framework, the downstream boundaries of storm tide predictions are provided by existing coastal guidance systems, whereas, streamflow forecasts at upstream rivers and local urban runoff are provided by the National Weather Service and the National Water Model. Additionally, high-resolution wind fields from the North American Mesoscale and the National Blend of Models are added to account for local wind effects on TWL. This model setup was successfully validated with a range of historical events and it also demonstrated improved forecast performance against the existing large-scale coastal guidance systems in a reforecast evaluation during 2020. Unlike other studies, we provided a comprehensive evaluation on the influence of individual flood drivers on TWL modeling and clearly demonstrated that the absence of one or more flood drivers in the model framework can underestimate simulated TWL in the National Capital Region.

1 **Title:** Integrated Coastal-River-Urban Total Water Level Forecast System for Tidal Rivers:  
2 Calibration, Validation, and Operational Evaluation

3

4 **Author names and affiliations:**

5 Arslaan Khalid<sup>1</sup>, Celso Ferreira<sup>1</sup>, Jason Elliott<sup>2</sup>

6 <sup>1</sup>Department of Civil, Environmental and Infrastructure Engineering, George Mason University

7 <sup>2</sup>NOAA/National Weather Service, Baltimore/Washington Forecast Office

8

9 **Corresponding author:**

10 Arslaan Khalid<sup>1,\*</sup>

11 <sup>1</sup> Department of Civil, Environmental and Infrastructure Engineering,

12 George Mason University, 4400 University Drive, Fairfax, VA 22030, USA

13 \*Corresponding Author: [akhalid6@gmu.edu](mailto:akhalid6@gmu.edu); Tel.: +1-703-678-9528

14

15 **Key Points:**

16 1. Ocean scale surge guidance systems underrepresent total water level in upstream tidal rivers  
17 in the Chesapeake Bay

18 2. Lack of river flows, urban runoff and local winds leads to inaccurate total water level  
19 forecasting

20 3. Ensemble-based total water level forecasting improved predictions for upstream tidal rivers

21

# 22 Integrated Coastal-River-Urban Total Water Level Forecast System for 23 Tidal Rivers: Calibration, Validation, and Operational Evaluation

24 Arslaan Khalid<sup>1</sup>, Celso Ferreira<sup>1</sup>, Jason Elliott<sup>2</sup>

25 <sup>1</sup>Department of Civil, Environmental and Infrastructure Engineering, George Mason University

26 <sup>2</sup>NOAA/National Weather Service, Baltimore/Washington Forecast Office

27

## 28 ***Abstract***

29 Existing real-time coastal flooding guidance systems in the US tend to underestimate total water  
30 level (TWL) predictions in upstream tidal areas of the Chesapeake Bay rivers, impacting flood  
31 forecasts for highly vulnerable areas, such as the National Capital Region. These under-predictions  
32 are mostly due to missing physical processes, lack of integration between hydrological and  
33 hydrodynamic models, and an oversimplification of the model setups used to predict TWL. In this  
34 study, an integrated TWL forecast system was introduced, where a high-resolution two-  
35 dimensional coastal storm surge model (ADCIRC) was implemented to simulate the combined  
36 influence of various flood drivers (storm tide, river flows, urban runoff, and local wind forcing) in  
37 the Potomac River. In this framework, the downstream boundaries of storm tide predictions are  
38 provided by existing coastal guidance systems, whereas, streamflow forecasts at upstream rivers  
39 and local urban runoff are provided by the National Weather Service and the National Water  
40 Model. Additionally, high-resolution wind fields from the North American Mesoscale and the  
41 National Blend of Models are added to account for local wind effects on TWL. This model setup  
42 was successfully validated with a range of historical events and it also demonstrated improved  
43 forecast performance against the existing large-scale coastal guidance systems in a reforecast  
44 evaluation during 2020. Unlike other studies, we provided a comprehensive evaluation on the  
45 influence of individual flood drivers on TWL modeling and clearly demonstrated that the absence  
46 of one or more flood drivers in the model framework can underestimate simulated TWL in the  
47 National Capital Region.

48

49 ***Keywords:*** ADCIRC; Flood Forecasts; Total Water Level; Washington, DC; Tidal Potomac.

50

51

## 52 ***1. Introduction***

53 Coastal metropolitan cities are dynamic and mostly located at the interface of multiple  
54 flood hazards (Depietri et al., 2018). These coastal communities are frequently hit by hurricanes  
55 and tropical storms in the US Atlantic and Gulf of Mexico coasts; therefore, subject to both heavy  
56 inland rainfall and coastal storm surge (Ray et al., 2011). The total global exposure from river and  
57 coastal flooding was estimated to be 46 trillion USD in 2010, with a probable increase of up to  
58 158 trillion USD by 2050 (Jongman et al., 2012). However, these floods are becoming increasingly

59 common in the tidal areas away from the open coast. Co-occurrence of different flood drivers in  
60 tidal areas like storm surges, river flow, rainfall-runoff, sea-level rise, and wind can result in  
61 increased water levels leading to compound floods (Herdman et al., 2018). The number of  
62 compound flooding events have increased significantly over the past century in many coastal cities  
63 (Wahl et al., 2015). Given an increase in flood events due to sea level rise (SLR) change (Atkinson  
64 et al., 2012; Zhong et al., 2008), as well as their intrinsic complexity in urban areas surrounding  
65 tidal rivers, accurate predictions of combined coastal-river-urban flooding are essential for cost-  
66 effective storm mitigation, emergency management plans, flood insurance, and planning. In 2019,  
67 for instance, one of the National Oceanographic and Atmospheric Administration (NOAA)  
68 monitoring station in the National Capital Region (Washington, DC) recorded water levels higher  
69 than the National Weather Service (NWS) “Action” flood level during portions of 195 days,  
70 compared to 150 days in 2017.

71 In some areas, the storm surge and wave components play the most important role in certain  
72 coastal flooding events; for others, the predominant component is the freshwater from the upstream  
73 river flow (Dresback, Fleming, Blanton, Kaiser, Gourley, Tromble, Luettich, Kolar, Hong, Cooten,  
74 et al., 2013). Co-occurrence of rainfall and coastal flooding can be more destructive, in contrast to  
75 if they occur separately (Ikeuchi et al., 2017). Exceptionally high tides, also called “King tide” in  
76 combination with slight storm surges can significantly increase the flooding potential in vulnerable  
77 areas (Loftis & Forrest, 2018). Atmospheric forcing (especially winds at 10m height) also play an  
78 important role in generating the local changes to water levels based on the station location and  
79 prevailing winds (Möller et al., 2001). Poor handling of storm water runoff by the community also  
80 results in increased volume of water entering the rivers (Walsh et al., 2012). Since these processes  
81 (surge, river flow, runoff and local winds) have a direct effect on the total water levels, absence of  
82 and variability in one or more physical processes directly leads to inaccurate estimates of total  
83 water levels (Lyddon et al., 2018). A comprehensive review of the studies of extreme flood events  
84 emphasized the importance of including multiple flood drivers (surge, river flow, runoff) in  
85 modeling tools for more accurate flood forecasts (Santiago-Collazo et al., 2019).

86 The lack of physical processes and its integration in the numerical modeling poses  
87 challenges for accurate total water level forecasting in real-time (Tshimanga et al., 2016). Current  
88 storm surge prediction methods are limited in their precision as they may regard tide and surge as  
89 separate processes, while completely ignoring the significance of a coupled tide-surge interaction  
90 (Bobanović et al., 2006). Additionally, fewer forecast systems extend the computational domain  
91 into shallower and narrower reaches of upstream rivers, leading to inaccurate hydrodynamic  
92 modeling in these areas. This simplification in the total water level forecasting is often adopted to  
93 avoid large computational costs related to high-resolution modeling in real-time environments  
94 (Ikeuchi et al., 2017). In addition to the simplification within the models, most of the models  
95 guidance and the NWS TWL forecasts are deterministic single-value outputs. In order to provide  
96 a better estimation of uncertainty and improving TWL accuracy, forecasters have also started  
97 considering ensemble forecasts. Furthermore, various studies investigated the influence of only

98 storm surge, or stream flows, or a combination of both on the water level modeling (J. Garzon &  
99 Ferreira, 2016; Herdman et al., 2018; Mashriqui et al., 2014; Svensson & Jones, 2004; Wahl et al.,  
100 2015; Wu et al., 2018; Zheng et al., 2013), therefore, a better understanding of the impact of flood  
101 drivers in TWL prediction needs to be developed for upstream tidal areas in complex estuaries.

102 The National Capital Region (NCR) of the US, located at the confluence of the Anacostia  
103 and the Potomac River, both of which are under the tidal influence of the Chesapeake Bay, is a  
104 perfect example of a region of national relevance that is impacted by compound flooding events  
105 (Sumi & Ferreira, 2019). Furthermore, existing flood guidance systems in operation underestimate  
106 the total water levels for the NCR area (Khalid & Ferreira, 2020). Even though the NWS issues  
107 watches and warnings for floods to protect life and property damage, the threat from flooding stays  
108 considerably high. The majority of forecast models currently in use do not integrate a range of  
109 forcing, such as river flows, urban runoff and local winds, to reflect compound events (Herdman  
110 et al., 2018). For instance, the existing two-dimensional (2D) or three-dimensional (3D) estuary-  
111 ocean models running at NOAA in an operational environment are one way coupled (Kourafalou  
112 et al., 2015) and do not account for observed or forecast freshwater in their calculations (Mashriqui  
113 et al., 2014). Additionally, the current unsteady flow models used by the NWS for riverine flood  
114 forecasting do not include the effect of urban runoff and local wind forcings (Mashriqui et al.,  
115 2014). While existing guidance systems provide the water level forecasts and the downstream  
116 boundary conditions for river scale forecasting, the simplification and lack of physical processes  
117 in the modeling framework results in significant underestimations (Herdman et al., 2018).

118 The objective of this study is to evaluate the interaction of coastal-river-urban processes  
119 that play an important role in real-time forecasting of compound flooding in tidal areas and  
120 demonstrate how the integration of these physical processes leads to an improved real-time TWL  
121 prediction in tidal rivers. Furthermore, the study aims to better understand the influences of storm  
122 surge, river discharge, urban runoff, and local winds on total water level predictions and provide  
123 recommendations for developing ensemble-based integrated total water level forecast systems for  
124 tidal rivers in large estuaries.

125

## 126 **2. *Methods***

127

128 In order to assess the relevance of an integrated framework for total water level modeling in  
129 upstream tidal areas, a dedicated hydrodynamic numerical modeling domain (section 2.2.2) was  
130 set-up for Potomac River. This framework was calibrated for accurate tidal modeling in the  
131 upstream tidal areas (section 2.2.3), where existing ocean scale coastal guidance systems mostly  
132 under-estimate extreme water levels under certain conditions. This calibration also focused on  
133 finding an optimal numerical mesh resolution that can allow high resolution modeling while  
134 keeping computational costs to a moderate level. The calibrated modeling framework was then  
135 validated against nine historical flooding events (section 2.3) to ensure model accuracy when

136 multiple flood drivers act simultaneously. We then focused on quantifying the change in water  
137 levels as a result of individual flood drivers' boundary conditions based on several hypothetical  
138 scenarios (section 2.4). Using real-time forecasted outputs from existing coastal and hydrologic  
139 guidance systems, we performed a reforecast test of several flooding events of 2020 within our  
140 integrated modeling framework to find the best set of boundary forcing for total water level  
141 forecasting (section 2.5). Lastly, through one case study, we demonstrated the system's ability to  
142 use ensemble based total water level forecasting (section 2.6) and assessed its performance against  
143 deterministic forecasting.

144

## 145 **2.1. Study Area**

146

147 The Potomac River is the largest tributary of the Chesapeake Bay, whose length from  
148 Washington, DC to the Chesapeake Bay is about 166 km. The tidal Potomac River is influenced  
149 by the tidal signal due to its downstream connection with the Chesapeake Bay. On the other hand,  
150 given the steep slope and the large incoming discharge, the water levels between Little Falls Pump  
151 Station (LFMD) and Chain Bridge are not tidally influenced, marking the end of the tidal signal  
152 influence in the river. The average daily flow at the LFMD is approximately 334 m<sup>3</sup>/s, whereas  
153 the maximum discharge of 13,705 m<sup>3</sup>/s (slightly greater than 100-year return period flow) was  
154 observed during the Great Flood of 1936. The Anacostia River joins the Potomac River in  
155 Washington DC, which is much shallower and narrower compared to the Potomac River  
156 (McDowell, 2016). Additionally, the average daily flow at the Anacostia River is as low as 4 m<sup>3</sup>/s,  
157 while the maximum measured discharge did not exceed 350 m<sup>3</sup>/s (less than 100 year return period  
158 flow). A number of small streams also flow into the Potomac River from Chain Bridge to  
159 Occoquan, with drainage areas ranging from 104 to 1554 square kilometers (km). The mean tidal  
160 range at Washington, DC is approximately 0.9 m while the tidal phase lags 5 h behind Lewisetta  
161 and 11.5 h behind that at Hampton Roads at the mouth of the Chesapeake Bay (NOAA tides and  
162 currents).

163

## 164 **2.2. Numerical Model Setup and Calibration**

165

### 166 *2.2.1. Advanced Circulation (ADCIRC) Hydrodynamic Model*

167

168 The Advanced Circulation (ADCIRC) model (Luettich et al., 1992) is a finite-element  
169 hydrodynamic model based on the generalized wave continuity equation (GWCE). These  
170 equations are solved on an unstructured computational grid in space and time to simulate the  
171 behavior of open water bodies like ocean, lake and rivers, forced by astronomical tides, coastal  
172 storms, and incoming river flows. It has been used extensively for modeling historical storm surges  
173 and forecasting flooding (Blain et al., 2010; Dresback, Fleming, Blanton, Kaiser, Gourley,  
174 Tromble, Luettich, Kolar, Hong, Van Cooten, et al., 2013; Funakoshi, Feyen, Aikman, Tolman,

175 Van Der Westhuysen, et al., 2012; Juan L. Garzon et al., 2018; Hanson et al., 2013; Shen et al.,  
176 2006). The two-dimensional, depth-integrated version of ADCIRC (ADCIRC-2DDI) is used in the  
177 barotropic mode to simulate the combined influence of astronomical tides, river inflows and storm  
178 surges on total water levels. ADCIRC is a FORTRAN-based open source numerical model and  
179 well documented, both in the published scientific literature (Luettich et al., 1992) and on the  
180 ADCIRC web site (<http://adcirc.org/>).

181

182

### 183 2.2.2. Numerical Mesh and Model Setup

184 The dedicated ADCIRC model grid developed for this study was constructed with  
185 upstream boundaries at Little Falls (USGS Station 01646500; latitude 38°56'59.2" longitude  
186 77°07'39.5"), MD, and the junction of Northeast and Northwest branch of Anacostia River, and a  
187 downstream boundary at Lewisetta, VA, as shown in **Figure 1**. The unstructured computational  
188 grid was developed using the automated mesh generator, OceanMesh2D (Roberts et al., 2019) for  
189 the ADCIRC model. This program allows the construction of varying resolution, project specific,  
190 numerical meshes in the area of interest. The high-resolution coastline from Global Self-consistent,  
191 Hierarchical, High-resolution Geography Database (GSHHG) (Wessel & Smith, 1996) was  
192 manually updated in the Potomac River to accurately represent the coastline in the numerical grid.  
193 The open ocean boundary was kept at Lewisetta as it allows the inclusion of the coastal boundary  
194 from this NOAA station or other forecast systems. Ocean boundary conditions for all the numerical  
195 experiments were provided by the NOAA predicted tides at the Lewisetta station to minimize the  
196 tidal prediction error resulting from low resolution Global Tidal Models. The topography and  
197 bathymetry datasets in our localized model were extracted from the USGS topographic Digital  
198 Elevation Model (DEM) and a set of other bathymetry sources (NOAA nautical charts (Austin,  
199 2005), NOAA National Centers for Environmental Information (NCEI) (Caldwell et al., 2015) and  
200 The Coastal National Elevation Database (CoNED) (Thatcher et al., 2016)) and a mosaic (Merged  
201 DEM) (detailed description on supplementary materials, section 1.2) with a vertical reference  
202 adjusted to North American Vertical Datum (NAVD88). In total five numerical meshes were  
203 developed using various nearshore and channel resolutions. Furthermore, four set of bathymetries  
204 (Modified NOAA nautical charts, NCEI, CONED and Merged DEM) were tested on ADCIRC  
205 numerical grids for model conveyance. The ADCIRC model was configured to run in explicit form  
206 of the barotropic mode. Wetting and drying, non-linear bottom friction, advection, finite amplitude  
207 terms, convective acceleration and the time derivative of convective acceleration were all included  
208 in the simulations. A detailed description of each recording station used in this study is provided  
209 in **Table A1** of appendix, while **Figure 1** shows the numerical modeling domain, several input  
210 boundary points and recording stations.



229 discrepancies (much shallower) compared to other regional bathymetry sources (NCEI and  
 230 CoNED); and 4) *manning's n* roughness value of 0.01 in open water presented smallest MAE in  
 231 modeled tides. The details on the methods and results of model calibration can be found in the  
 232 supplementary materials (section 1 and 3.1).

233

234 **Table 1.** Model calibration parameters used for astronomical tides modeling in ADCIRC

235

<b>Parameters</b>	<b>Test1</b>	<b>Test2</b>	<b>Test3</b>	<b>Test4</b>
<i>Bathymetry Datasets</i>	Modified NOAA nautical charts	NCEI	CONED	Merged DEM
<i>Numerical Model Resolution</i>	Low resolution with no defined channels	Low resolution with defined channels	High resolution with no defined channels	High resolution with defined channels
<i>Bottom Friction (Manning's)</i>	0.02	0.018	0.015	0.01
<i>Horizontal Eddy Viscosity (m<sup>2</sup>/s)</i>	0.5	1	5	10

236

237

238

239 **2.3. Validation Cases**

240

241

242

243

244

245

246

247

248

249

250

251

252

253

254

255

256

257

258

A number of historical case studies (9 in total) are used to validate the integrated numerical modeling framework using the calibrated parameters referenced in section 2.2.3. These case studies consist of three historical events for each flooding source type: River, Coastal, and Compound. A flood event is classified as a “River” driven flood if the increase in the water at WASD is majorly influenced by the upcoming discharge from the river (LFMD) leading to water levels above the NWS defined “Action” stage at WASD. A “Coastal” driven flood event is defined as the result from a strong storm surge signal from LWTV that travels upstream and a relatively low discharge from upstream (LFMD). A “Compound” flood is defined when a combination of both high river discharge and high coastal water levels occur at the same time. Three major input forcings are used based on the availability of the observed data: downstream water levels, upstream major river discharges, and WASD wind spread spatially over the modeling domain. The downstream boundary is retrieved from the observed water levels at LWTV, but in cases where observed water levels are not available for LWTV, data from Sewells Point (SWPV) is used and adjusted for the amplitude and timing of LWTV (-5 h). The upstream discharge boundary is provided by the daily-observed flow at Little Falls, which is interpolated to hourly flow using a spline interpolation. The wind data was not available for WASD station prior to 2008, and therefore, the observed wind data from LWTV was used for case studies after 1973 as an approximation. For model validation prior to 1973, no wind forcing was used. It must

259 be noted that due to data interpolation and using proxy data in the absence of observed data, some  
 260 uncertainty can propagate in the model results. All these model validations were simulated for  
 261 nearly 23 days, starting at least 10 days prior to observed maximum water levels at the WASD  
 262 station to allow the model to warm up and increase stability. A detailed description for data  
 263 availability of each case study is given in **Table 2** and the time series of observed data is shown  
 264 in **Figure A2** of appendix. Additionally, the detailed description of each historical event used in  
 265 the model validation is provided in the supplementary materials (section 2).

266  
 267

268 **Table 2.** Case studies for model validation

Sr. No	Events	Type	Year	Dates	DC max (m)	Observed Water			Observed Flow	Observed Winds
						WASD	LWTV	SWPV	LF	LWTV or WASD
1.	<i>Great flood of 1936</i>	River	1936	03/14-03/24	2.79	Y	N	Y	Y	N
2.	<i>Blizzard of 1996</i>	River	1996	01/14-01/25	2.04	Y	Y	Y	Y	Y
3.	<i>Hurricane Agnes</i>	River	1972	06/10-06/02	2.22	Y	N	Y	Y	N
4.	<i>Flood of 1937</i>	Compound	1937	04/22-05/02	2.18	Y	N	Y	Y	N
5.	<i>Hurricane Fran</i>	Compound	1996	09/04-09/15	2.04	Y	Y	Y	Y	Y
6.	<i>Hurricane Isabel</i>	Compound	2003	09/15-09/27	2.7	Y	Y	Y	Y	Y
7.	<i>TS Ernesto</i>	Coastal	2006	08/28-09/05	1.61	Y	Y	Y	Y	Y
8.	<i>Hurricane Sandy</i>	Coastal	2012	10/20-11/11	1.44	Y	Y	Y	Y	Y
9.	<i>Hurricane Florence</i>	Coastal	2018	09/05-09/20	1.48	Y	Y	Y	Y	Y

269

270  
 271

## 272 **2.4. Influence of Input Boundary Conditions and Atmospheric Forcing**

273

274 In order to investigate the effects of different flood drivers on the total water level in the  
 275 Potomac River, a comprehensive sensitivity analysis was performed on scenarios representing a  
 276 range of: 1) downstream boundary conditions (i.e., storm surges); 2) upstream boundary  
 277 conditions (i.e., major river discharges); 3) additional lateral boundary conditions (local urban  
 278 runoff); 4) combined upstream and lateral boundary conditions; and 5) surface wind forcing at  
 279 the local scale. For each scenario, we ran the simulation for 15 days including 3 days for spin-up  
 280 time and compared with a baseline tides only simulation. Note that the change in water levels as  
 281 a result of certain flood driver at the recording stations is presented as “above normal daily tides”,  
 282 which is referred to a full tidal cycle including one high and one low tide.

283 When analyzing the influence of downstream boundary conditions on the change in total  
284 water levels at WASD, a set of storm surge simulations were performed, where downstream peak  
285 storm surge signal based on various return periods at LWTV defined by NOAA was applied. The  
286 peak surges were estimated at 0.956 m, 1.106 m, 1.236 m, and 1.346 m above NAVD88 datum  
287 at LWTV for 10, 25, 50, and 100 year, respectively. To minimize the influence from other flood  
288 drivers, no stream flow or local wind forcing was included. Whereas, to quantify the change in  
289 water levels resulting from upstream major river flows, we performed a set of simulations with  
290 flows ranging from 25 to 100 year return period. These flows are based on USGS StreamStats  
291 analysis (Ries III et al., 2017) and provided in **Table 3**. Apart from upstream river discharges, we  
292 also introduced urban runoff in the ADCIRC model at various streams along the Potomac River  
293 (**Figure 1**) and took a similar approach based on design stream flows (25 to 500 year return  
294 periods) for quantifying change in water levels. These stream flows differ from the major river  
295 flows, as they flow laterally and represent the water added to the Potomac River in case of heavy  
296 rainfall in the surrounding watersheds. Additionally, we performed a set of simulations with  
297 combined flows from major rivers (upstream) and urban runoff to quantify the change in water  
298 levels when both are contributing to Potomac River flow. Lastly, for investigating the effect of  
299 local winds on the water level variations at WASD, we performed a set of tests with local wind  
300 forcing. We reproduce eight wind directions (N, NE, E, SE, S, SW, W, and NW) with magnitudes  
301 ranging from 5-35 m/s for 12 hours, based on the observed data at WASD (2008-2020). The  
302 predominant winds observed at WASD are from NW and S. Additionally, historical NOAA  
303 records show winds from SE greater than 40 m/s and winds from NW nearly 35 m/s at Dulles  
304 Airport station (IAD) have been recorded. **Figure A2** in appendix shows a wind rose of observed  
305 wind speeds and direction at WASD.

306  
307  
308 **Table 3.** Flow characteristic for major rivers and urban runoffs  
309

	Full name	Code	Drainage Area (km <sup>2</sup> )	Max measured flow (m <sup>3</sup> /s)	Min measured flow (m <sup>3</sup> /s)	Average daily flow (m <sup>3</sup> /s)	25yr return period	50yr return period	100yr return period
<i>Major Rivers</i>	Little Falls at Potomac River	LFMD	29940	13705	17	334	8680	10752	12908
	Bladensburg at Anacostia River	BDMD	239	349	0	4	233	317	580
<i>Urban Runoffs</i>	Rock Creek	RoCrk	521	77	0	2	330	417	518
	Oxon Run	OxCrk	98	-	-	-	121	160	209
	Four Mile Run	FMRun	122	36	0	0	308	390	483
	Broad Creek	BrCrk	173	35	0	1	166	218	283
	Piscataway Creek	PiCrk	420	127	0	1	231	300	384
	Little hunting Creek	LiHuntCrk	65	-	-	-	23	31	39
	Occoquan Creek	OxCrk	1538	784	0	14	623	759	921
	Cameron Run	CMRun	228	116	0	1	349	426	512

311

312 The forcing used in these scenarios are hypothetical and reflect the simplified versions of  
313 the real cases from normal daily weather to extreme weather conditions. These scenarios will  
314 allow us to better characterize contribution of each flood driver on total water levels and highlight  
315 the importance for inclusion or exclusion in a real-time integrated modeling framework.

316

317

## 318 **2.5. Investigation of Operational Boundary Conditions for Real-Time Total Water Level** 319 **Forecasting**

320

321 Here, we discuss the various operational guidance systems (hydrometeorological and  
322 hydrodynamic) currently available that provide forecasted boundary forcing (downstream, major  
323 river flows, urban runoff and local winds) for total water level forecasting in the region. First, the  
324 original forecasts from the guidance systems were compared against observations to assess  
325 individual forecast bias. A set of events (*River, Coastal* and *Compound*) from the year 2020 were  
326 used as a test-bed to evaluate the real-time total water level forecasts using these predicted outputs.  
327 Since these events are reforecasted, we used the average of all the real-time forecasts issued daily  
328 (six hourly cycles). The time series of observed data for these reforecast events are shown in  
329 **Figure A3**, while **Table 4** provides the set of available guidance systems for various boundary  
330 types.

### 331 *2.5.1. Downstream Boundary Conditions*

332 The downstream boundary condition for forecasting the water levels in the Potomac River  
333 can be provided from a number of sources, including but not limited to global tidal prediction  
334 models (TPXO (Egbert & Erofeeva, 2002)), NOAA predicted astronomical tides, official water  
335 level forecasts from NWS or water level guidance provided by continental-scale storm surge  
336 guidance systems (Extra Tropical Storm Surge (ETSS) (Kim et al., 1996), Extratropical Surge  
337 and Tide Operational Forecast System (ESTOFS) (Funakoshi, Feyen, Aikman, Tolman, van der  
338 Westhuysen, et al., 2012), Chesapeake Bay Operational Forecast System (CBOFS) (Gross et al.,  
339 2000), integrated FLOOD Forecast System (iFLOOD) (Khalid & Ferreira, 2020), bias corrected  
340 iFLOOD water level (iFLOODv2) (Khalid & Ferreira, 2020) and Ensemble of all guidance  
341 systems) at LWTV station. The NOAA-predicted astronomical tides at LWTV provide an  
342 accurate estimate of astronomical tidal variation at LWTV, while the NWS or other guidance  
343 systems provide water levels that include a combination of storm surge and astronomical tides.  
344 We compared the forecasted water levels by various guidance systems and NWS against the  
345 observed water levels at LWTV (Jan 2020 to Aug 2020) to evaluate the best performing  
346 downstream boundary conditions for simulating total water levels in WASD during the reforecast  
347 *Coastal* event of 2020.

348

### 349 *2.5.2. Upstream Boundary Conditions of Major River Flows*

350 Currently, the NWS and the National Water Model (NWM) are the only sources that can  
351 provide the upstream river discharge boundaries (**Figure A4**) in real time for the Potomac River.  
352 The NWS stream flow forecasts are produced by the Middle Atlantic River Forecast Center  
353 (RFC), but are only provided at major discharge locations such as Little Falls (LFMD). NWS  
354 forecasts are only available for up to 72 hours in the future for these locations. No flow  
355 predictions are available from the RFC for the Anacostia River confluence (BDMD). The NWM,  
356 which is a continental scale hydrologic prediction system (Cosgrove et al., 2018), also provides  
357 flow forecasts for a number of timescales (Short, Medium and Long range) over a national  
358 coverage of nearly 2 million reaches. The NWM stream flow from the Medium range forecasts  
359 are available at LFMD and BDMD, and are used as upstream boundaries for major river flows.  
360 Since these flows influence the *River* and *Compound* events primarily, we used NWS and NWM  
361 forecasts as upstream boundaries to determine the best performing upstream boundary condition  
362 model. Note that we only analyzed the upstream boundary conditions for *River* events.

### 363 2.5.3. *Upstream boundary conditions of Urban Runoff*

364 As noted, the RFC does not provide flow forecast for all the streams in the region, and  
365 therefore the NWM is the only forecast source for almost all the urban streams (shown in **Figure**  
366 **A4**) in the region. The NWM stream flow forecasts were compared against the available USGS  
367 stream flow gages to understand the forecast bias. For the test period in 2020, no major urban  
368 flood event significantly affected total water levels at the WASD station; therefore, we could not  
369 validate the additional value of including the urban runoff boundary from the streams during the  
370 period. However, we used the NWM forecasted stream flows during the *Compound* reforecast  
371 event (April 2020) to analyze change in total water levels.

### 372 2.5.4. *Atmospheric Forcing for Local Winds*

373 Although a number of weather models are available for our study area, we limited our  
374 scope of evaluation for two forecasted model outputs only, North American Mesoscale (NAM)  
375 12 km resolution and National Blend of Models (NBM) 2.5 km. In contrast to NAM, NBM is not  
376 a numerical model, instead it is a blended dataset based on NWS and non-NWS numerical weather  
377 prediction models. At least two studies (J. L. Garzon et al., 2018; Khalid & Ferreira, 2020) have  
378 shown that NAM is a highly skillful model for wind forecasts in the Chesapeake Bay, however,  
379 a NBM evaluation is not established for this region. Here we tested the accuracy in simulating the  
380 local wind impacts to total water levels based on these two wind models during a *Compound*  
381 reforecast event (April 2020). The forecasted wind speeds and direction at 10 m height were  
382 specified on the numerical modeling grid to simulate local wind impacts.

383

384

385 **Table 4.** Available boundary conditions for real-time total water level forecasting in  
386 Potomac River

<b>Boundary Types</b>	<b>Forecast/Guidance System</b>
<i>Downstream Water Levels</i>	NWS/ETSS/CBOFS/ESTOFS/iFLOODv2/iFLOOD
<i>Upstream Major River Flows</i>	NWS/NWM
<i>Upstream Urban Runoff</i>	NWM
<i>Atmospheric Forcing</i>	NAM(12km) /NBM(2.5km)

387

388

## 389 2.6. Ensemble Based Forecasting

390 Based on the available set of guidance systems mentioned in Table 4, we devised a full set of  
391 ensembles (> 30) containing various combinations of model input boundary forcing (downstream,  
392 upstream, urban and local winds) to simulate ensemble-based total water level forecasts. However,  
393 we then lowered the total number of ensembles to a maximum of 10 members based on the best  
394 performing guidance system for model input forcing. This set consisted of 5 downstream (CBOFS,  
395 ETSS, NWS, iFLOODv2, Ensemble), 1 upstream (NWS), 2 local wind forcing (NAM, NBM) and  
396 1 urban runoff (NWM) boundary. In order to gain computational efficiency, we used a low-  
397 resolution mesh with defined dredged channels (*low\_ch*, detailed in supplementary materials,  
398 section 1.1), therefore, the quality of the modeled total water levels was limited by the finite  
399 resolution of the model. However, it provided computational speed, while maintaining an  
400 integrated framework. These ensemble simulations were initialized from the existing deterministic  
401 forecast system for Chesapeake Bay. Our analysis of the ensemble forecasting in the Potomac  
402 River is also based on the *Compound* reforecast event of 2020. The different types of ensemble  
403 forecasts are summarized in Table 5.

404

405

406

**Table 5.** Summary of ensemble configurations

<b>Abbreviation</b>	<b>Upstream</b>	<b>Downstream</b>	<b>Urban Drainage</b>	<b>Atmospheric Forcing</b>
<i>Ens1</i>	NWS	ETSS	NWM	NAM (12km)
<i>Ens2</i>	NWS	CBOFS	NWM	NAM (12km)
<i>Ens3</i>	NWS	NWS	NWM	NAM (12km)
<i>Ens4</i>	NWS	iFLOODv2	NWM	NAM (12km)
<i>Ens5</i>	NWS	Ensemble	NWM	NAM (12km)
<i>Ens6</i>	NWS	ETSS	NWM	NBM (2.5km)
<i>Ens7</i>	NWS	CBOFS	NWM	NBM (2.5km)
<i>Ens8</i>	NWS	NWS	NWM	NBM (2.5km)

<i>Ens9</i>	NWS	iFLOODv2	NWM	NBM (2.5km)
<i>Ens10</i>	NWS	Ensemble	NWM	NBM (2.5km)

---

407

408

### 409 3. Results and Discussion

410

411

#### 412 3.1. Model Validation

413

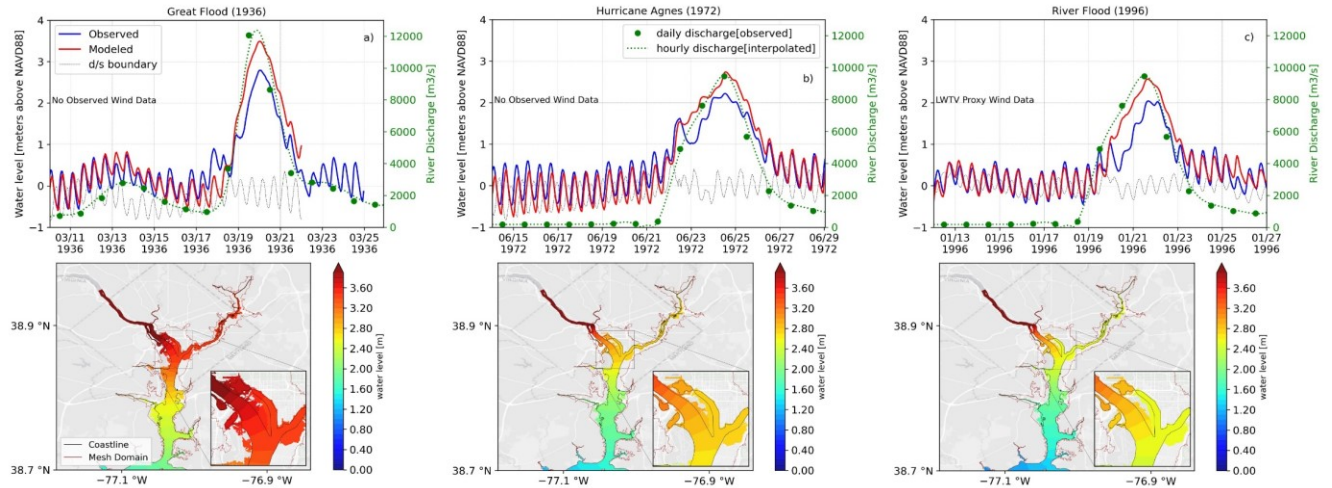
414 The ADCIRC model setup used in this study, including a combination of three boundary  
 415 forcings (downstream water levels, upstream discharge and local winds) is validated on the high-  
 416 resolution numerical mesh with overland areas (*high\_OL*) using nine historical events  
 417 (supplementary materials, section 3.1.2).

418

##### 419 3.1.1. Historic Riverine Events

420 The historical validation of the extreme *River* events was predominantly dependent on the  
 421 accuracy of the upstream flow observed boundary. The time series of simulated total water levels  
 422 (TWL) against the observations at the WASD station are shown for all the three riverine events in  
 423 **Figure 2**. The model simulated the increase in TWL as a result of large river discharge from  
 424 LFMD, however, the modeled peak was 0.5 m larger than the observed peak. The simulated TWL  
 425 during the 1936 Flood show an increase of 3 m above normal daily tide as a result of an  
 426 approximate 100-year return period flow recorded at LFMD station. Based on upstream river flow  
 427 analysis as shown in **Figure 6**, 100-year return period flow can increase the water level at WASD  
 428 by almost 3.6 m; however, that increase is estimated when both upstream boundaries are flooding  
 429 simultaneously. Historical simulation of Hurricane Agnes in 1972 and River Flood of 1996 also  
 430 showed the same over prediction of 0.5 m at the WASD station. Note that these simulations do not  
 431 include the local wind effects, as no observed wind data at WASD before 2008, and according to  
 432 **Figure 8**, local wind can impact the water levels by  $\pm 0.5$  m above normal daily tide when wind  
 433 speeds are nearly 15 m/s. Additionally, the lower panels of **Figure 2** shows the inland extent of  
 434 flooding during these three river events.

435



436

437 **Figure 2.** Time Series of total water level (TWL) and spatial map of maximum TWL during the  
 438 peak of storm at WASD a) Great Flood (1936) b) Hurricane Agnes (1972) c) Blizzard (1996)

439

440

441 *3.1.2. Historic Coastal Events*

442

443

444

445

446

447

448

449

450

451

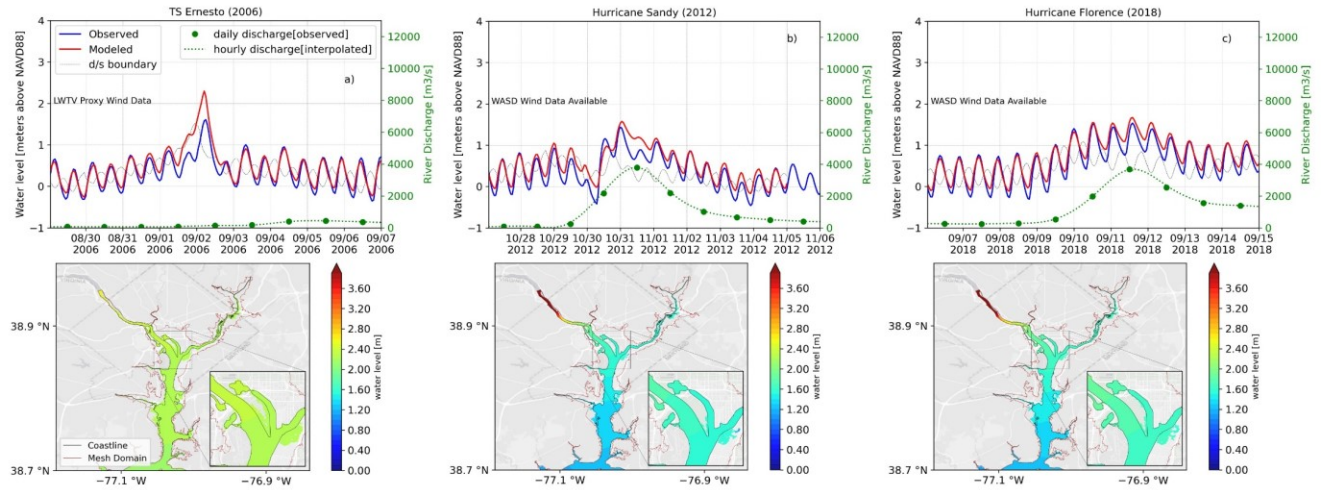
452

453

454

455

The historical validation of the *Coastal* events, on the other hand, is majorly dependent on the accuracy of the downstream water level boundary and atmospheric forcing. The time series of simulated TWL against the observations at the WASD station are shown for all the three coastal events in **Figure 3**. The model simulated the increase in TWL at the WASD station as a result of strong storm surge signal propagating upstream from LWTV. The time series of the modeled peak at WASD was over estimated by 0.5 m for Tropical Storm Ernesto (2006), while in case of Hurricane Sandy (2012) and Florence (2018), the model captured the peak more accurately. During TS Ernesto, no observed wind data was available at WASD, and instead proxy data from LWTV was used. Since local winds have potential to impact water levels by  $\pm 0.5$  m above normal daily tide when wind speeds are nearly 15 m/s (**Figure 8**), inaccurate wind data used during simulation could have resulted in noted overestimations. The section 3.2.4 further elaborates the local changes in water levels at a recording station due to local wind effects. Similar to **Figure 2**, **Figure 3** also shows the extent of flooding during these three *Coastal* events, which is not propagated overland as far as *River* based events.



456

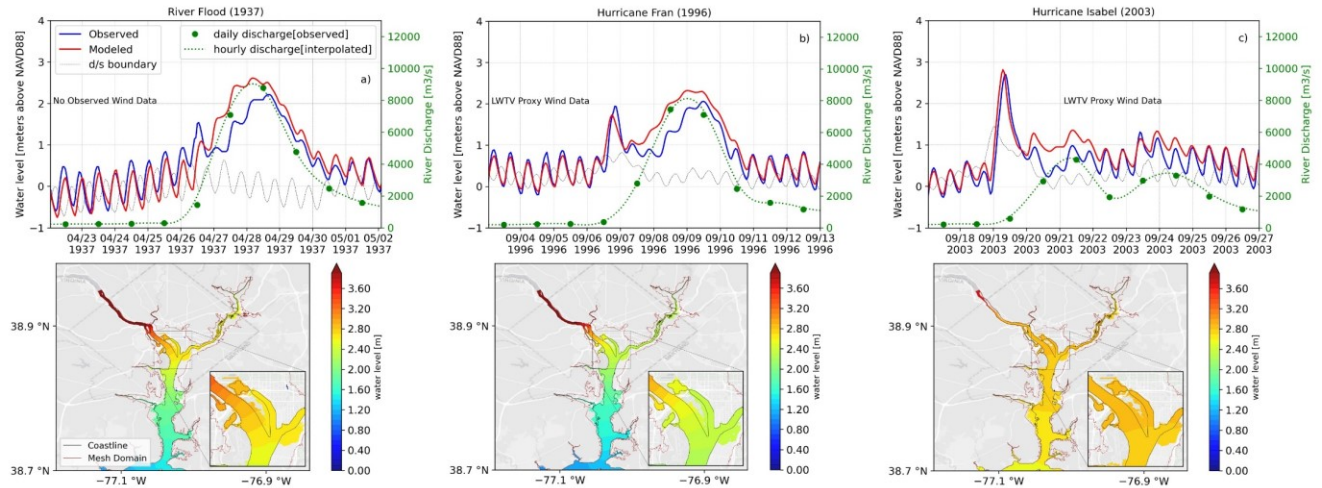
457 **Figure 3.** Time Series of TWL and spatial map of maximum TWL during the peak of storm at  
 458 WASD a) TS Ernesto (2006) b) Hurricane Sandy (2012) c) Hurricane Florence (2018)

459

460 *3.1.3. Historic Compound Events*

461 The time series of TWL results from simulations of three major *Compound* events that  
 462 happened in the National Capital Region are shown in **Figure 4**. The simulated results show that  
 463 the model was able to reproduce the first peak of the compound events (exception of River Flood  
 464 1937) more accurately when compared to the second peak that was influenced by a large upstream  
 465 river discharge at LFMD. Among all the three case studies, the first peak at the WASD was  
 466 correctly modeled during Hurricane Isabel (2003) and Hurricane Fran (1996). Interestingly, the  
 467 second peak followed by the large upstream flow showed an overestimation of 0.5 m during all  
 468 the three events, similar to *River* and *Coastal* events validations. Similarly, since no observed wind  
 469 data was available for WASD during all these three *Compound* events, one can argue that accurate  
 470 local atmospheric forcing could help with accurate estimations of TWL.

471



472

473 **Figure 4.** Time Series of TWL and spatial map of maximum TWL during the peak of storm at  
 474 WASD a) River Flood (1937) b) Hurricane Fran (1996) c) Hurricane Isabel (2003)

475

476 Furthermore, a consistent over prediction of 0.5 m was noted during high upstream river  
 477 discharges. Our validation results for Great Flood of 1936 and Hurricane Isabel (2003) at WASD  
 478 showed slight discrepancy from the results published in an earlier study (Wang et al., 2015), where  
 479 the authors used a Semi-implicit Cross-scale Hydroscience Integrated System Model (SCHISM)  
 480 with upstream river boundary at LFMD and downstream boundary at Colonial Beach. The  
 481 simulated peak of our modeling setup showed 0.5 m overestimation during Great Flood of 1936,  
 482 but only a 0.1 m over prediction during Hurricane Isabel peak. Simulated water level peak error  
 483 during Isabel also compared favorably with ADCIRC model results at WASD published earlier  
 484 (Mashriqui et al., 2014). It is worthwhile to note that the model tends to overestimate TWL by  
 485 almost 0.5 m when stream flows higher than 3000 m<sup>3</sup>/s are introduced at the LFMD boundary.  
 486 Additionally, for some historical events, some of the observed data (LWTW water levels and  
 487 WASD winds) were not available, which may have led to uncertainty in the simulated water levels.  
 488 Lastly, the Potomac River channel has undergone significant changes since the 1930s that may  
 489 have also influenced the simulated results at WASD. This becomes clear upon examination of the  
 490 model validation results that the integrated modeling framework can simulate historic extreme  
 491 water levels at WASD with slight over predictions (~0.5 m). Since the over prediction was  
 492 consistent in all the case studies, proposed a systematic bias correction at WASD when Potomac  
 493 River flows are above 3000 m<sup>3</sup>/s to increase the accuracy of model results.

494

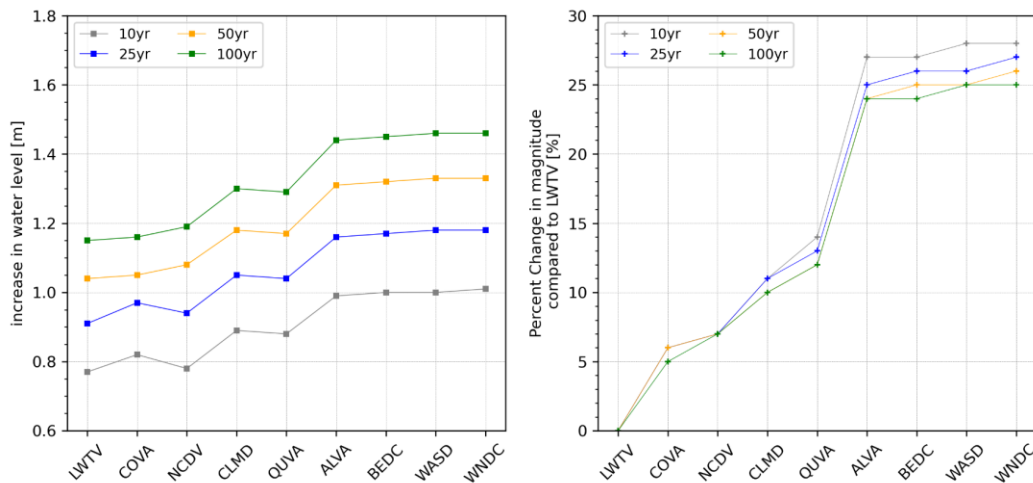
495

### 496 3.2. Influence of Input Boundary Conditions and Atmospheric Forcing

497

#### 498 3.2.1. Downstream Boundary Conditions

499 **Figure 5** shows the increase in water levels above normal daily tides at a number of  
500 recording stations (LWTV to WASD), when 10 to 100 year return period storm surge enters the  
501 Potomac River. The growth in magnitude becomes consistent at Alexandria (ALVA) and continues  
502 upstream. Results show that maximum increase in water levels above normal daily tides at WASD  
503 during a 100-year return period does not exceed 1.5 m. TS Ernesto in 2006 resulted in a similar  
504 magnitude of surge propagating upstream from LWTV (1.468 m above NAVD88) and elevated  
505 the water levels at WASD by almost 1.11 m above NOAA predicted astronomical tides. The  
506 discrepancy between the estimated increase and observed increase due to downstream boundary  
507 conditions could have resulted from other flood drivers during TS Ernesto. Results also show that  
508 there is almost a 26% increase in storm surge magnitude (right panel of **Figure 5**) as the storm  
509 surge signal travels from LWTV to WASD. Historical data analysis (Sumi & Ferreira, 2019)  
510 demonstrated that LWTV contributes 80% of the water level in WASD, whereas we found almost  
511 76% in this analysis. Since such a large contribution of water level exists due to downstream  
512 boundary condition, it is very important for accurately estimating total water level.  
513



514  
515 **Figure 5.** Change in water levels magnitude (above normal daily tides) in the Potomac  
516 River due to downstream boundary conditions.  
517

518  
519 *3.2.2. Upstream Boundary Conditions of Major River Flows*

520 **Figure 6** shows the increase in water levels when a range of return period (25 to 100 year)  
521 discharges are introduced on a normal tidal simulation in January 2020. The increase resulting  
522 from individual upstream rivers discharges is also show as dashed and dotted lines in **Figure 6**.  
523 Since the drainage area for the Anacostia River is significantly smaller, the increase in water level  
524 based on Anacostia discharges were almost negligible for 25 to 100 year return period discharges.  
525 Whereas, Potomac River discharges raised water levels nearly 4 m above normal river elevation  
526 during a 25-year return period at WADC, which surpassed 5.5 m mark as the return flow increased

527 to 100-year return period. It is interesting to note that the increase in water levels at the WASD  
528 station as a result of 25 and 100-year return period is almost 2.5 to 4 m above normal daily tides.  
529 Our model validation for the 1936 Flood showed slightly smaller increase in water level (~3 m  
530 above normal tides) at WASD when a 100-year observed return period flow at LFMD flooded the  
531 region. Note that during validation for the 1936 Flood, only LFMD exceeded the 100-year return  
532 period flows, while BDMD had no record of observed flow until 1938. **Figure 6** also shows the  
533 increase in water level as a function of distance when various return period flows were introduced.  
534 The plot suggests that upstream discharge can have an influence as far downstream as Colonial  
535 Beach (COVA), which aligns well with the observation in Mashriqui's study (Mashriqui et al.,  
536 2014).. This analysis showed the importance of including the upstream major discharge  
537 boundaries, since in the absence of upstream boundaries, the model will not be able to capture  
538 TWL, especially when riverine flows are above 10 times average daily flow (equivalent to 2 year  
539 return period).

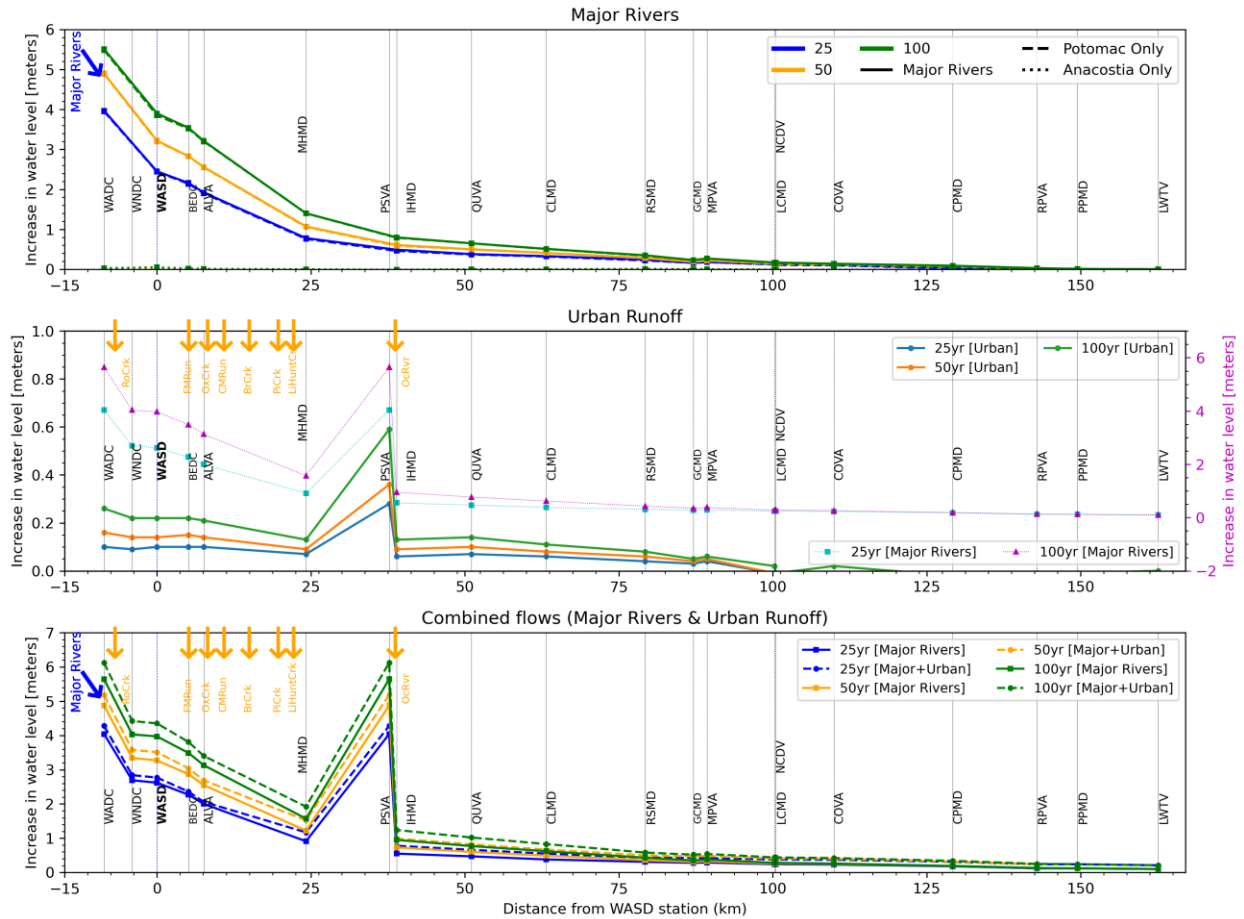
540

### 541 *3.2.3. Upstream Boundary Conditions from Urban Runoff*

542 The second panel of **Figure 6** shows the increase in water levels when a range of return  
543 period stream flows from tributaries (yellow arrows in **Figure 1**) are introduced in the Potomac  
544 River. It can be seen that the increase in water levels is not as prominent as the results caused by  
545 major river flows (25-year return period flow by major river is added as reference in second panel  
546 of **Figure 6**); however, stations close to the stream boundaries experienced an increase of water  
547 level between 0.22 m to 0.59 m above normal daily tides during a 100-year return period flow.  
548 Rock Creek, which is upstream of the WASD station, in the absence of major river discharge, only  
549 increased the water levels by 0.22 m above normal daily tides during a 100-year return period  
550 flow.

### 551 *3.2.4. Upstream Boundary Conditions from Combined River flows and Urban Runoff*

552 Additionally, we performed a set of simulations with combined major river flow and urban  
553 runoffs for 25-100 year return period flows. The lowest panel of the **Figure 6** shows the increase  
554 in water levels above normal daily tides as function of distance while arrows on the figure also  
555 indicate the location of various streams and Major River inputs. Interestingly, the increase in water  
556 level as a result of combined major river flow and urban runoff for 100 year return period raise by  
557 almost 0.4 m and becomes equal to a 200 year return period (not shown here) during a major river  
558 flow only. Similarly, the increase in water levels at WASD as a result of combined discharges for  
559 100 year exceeds the 4.35 m height above normal daily tides. This analysis shows the importance  
560 of including the urban drainage in addition to major river flows when modeling historical events  
561 or developing an integrated total water level forecast system. Although urban runoff boundary  
562 alone may not influence the water levels significantly at WASD, when combined with large river  
563 discharge, it will significantly impact simulated TWL.



564

565 **Figure 6.** Change in water levels above normal daily tides in the Potomac River due to  
 566 major river, urban runoff and combined discharges boundary conditions

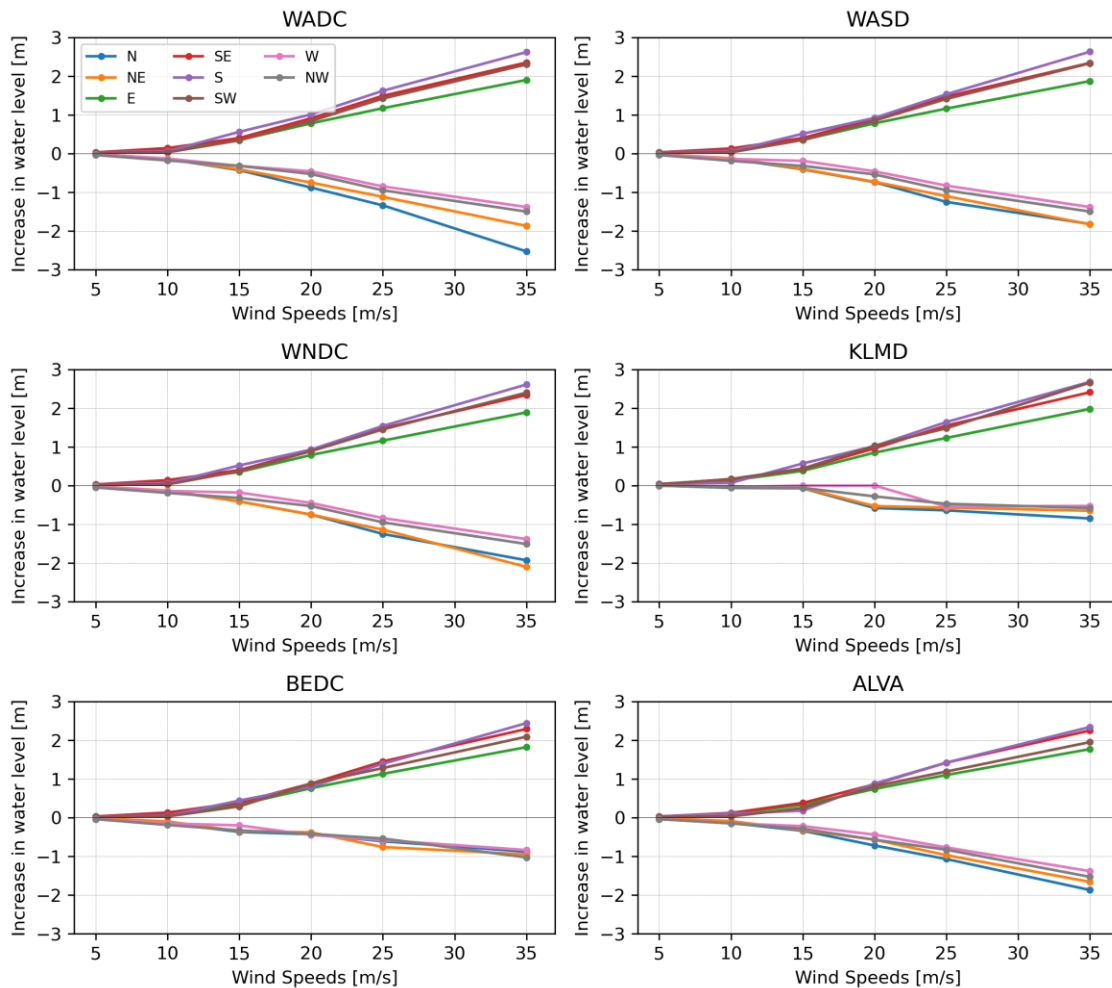
567

568

569 *3.2.5. Effect of Local Winds*

570 The results of considering local effects of winds for eight primary directions at six stations  
 571 surrounding WASD are shown in **Figure 7**. The positive values of change show an increase in  
 572 water levels, while negative values show a decrease in water levels. Based on the location of the  
 573 WASD recording station, we would expect an increase in water levels locally when winds are  
 574 blowing from South and a decrease in water levels when wind blowing from NW (pushing water  
 575 away from the station). **Figure 7** clearly shows that when winds are blowing from N, NE, W and  
 576 NW direction they tend to decrease the water levels at the WASD station and as the magnitude of  
 577 the winds increase, a large decrease is shown. An opposite trend is noted when winds are blowing  
 578 from S, SW, E and SE. These local changes to total water levels as a result of local winds are  
 579 shown in an earlier study using a Delft3D model, where winds >5.5 m/s from NW direction drained  
 580 water out of Potomac River, therefore lowering the water levels at WASD (Mashriqui et al., 2014).  
 581 Our wind forcing analysis showed the importance of including local wind forcing in excess of 5.5

582 m/s to accurately capture the changes to total water level locally. On the other hand, winds smaller  
 583 than 5.5 m/s will not affect the water levels locally, therefore forecasts produced by ocean scale  
 584 coastal guidance systems by ignoring local winds will perform similar to our dedicated Potomac  
 585 forecast system. Analysis of observed winds at WADC showed that magnitudes between 5 m/s and  
 586 8 m/s are observed at least once in most months (**Figure A5** in appendix). Although events with  
 587 local wind speeds greater than 10 m/s (**Figure A5** in appendix) are less common, the absence of  
 588 local wind forcing in such events, will completely misrepresent the forecasted TWL.

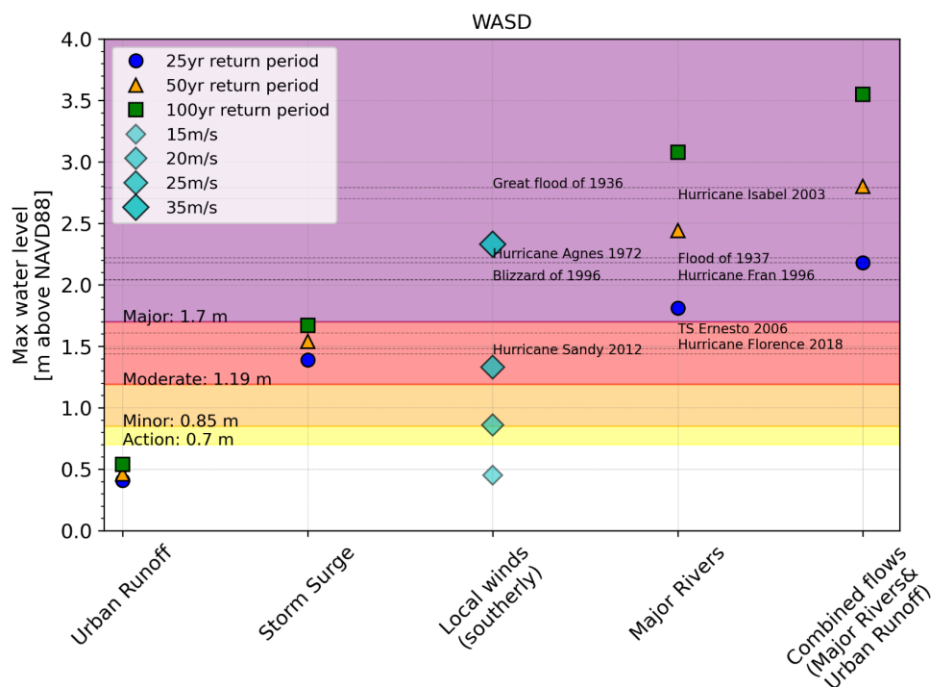


589  
 590 **Figure 7.** Change in water levels above normal tides at WADC and nearby stations due  
 591 to local winds forcing in eight directions.  
 592

593  
 594 *3.2.6. Summary of flood driver's influence*  
 595

596 **Figure 8** provides a summary for the relevance of individual flood drivers at WADC. Note  
 597 that the systematic error (+0.5 m) at WADC noted during the validation of historic river events  
 598 (section 3.1.1) is corrected when estimating the maximum water levels shown in **Figure 8**. The

599 urban runoff boundary does not increase the water levels above “Action” stage as a result of 25 to  
 600 100 year return period. Storm surges, on the other hand, can increase the maximum water levels  
 601 at WASD above “Moderate” flooding level, i.e. as noted during TS Ernesto 2006. Local wind  
 602 forcing greater than 20 m/s from South direction is also shown here to increase the maximum water  
 603 levels from “Minor” to “Major” flooding level. Among all the individual flood drivers, major  
 604 rivers discharges of 100-year return period are shown to cause the maximum water levels at  
 605 WASD, i.e. as noted during Great Flood of 1936. Lastly, maximum water levels caused by  
 606 combined river flows provides an example of combination of flood drivers that leads to significant  
 607 influence on the water levels at a given recording station.

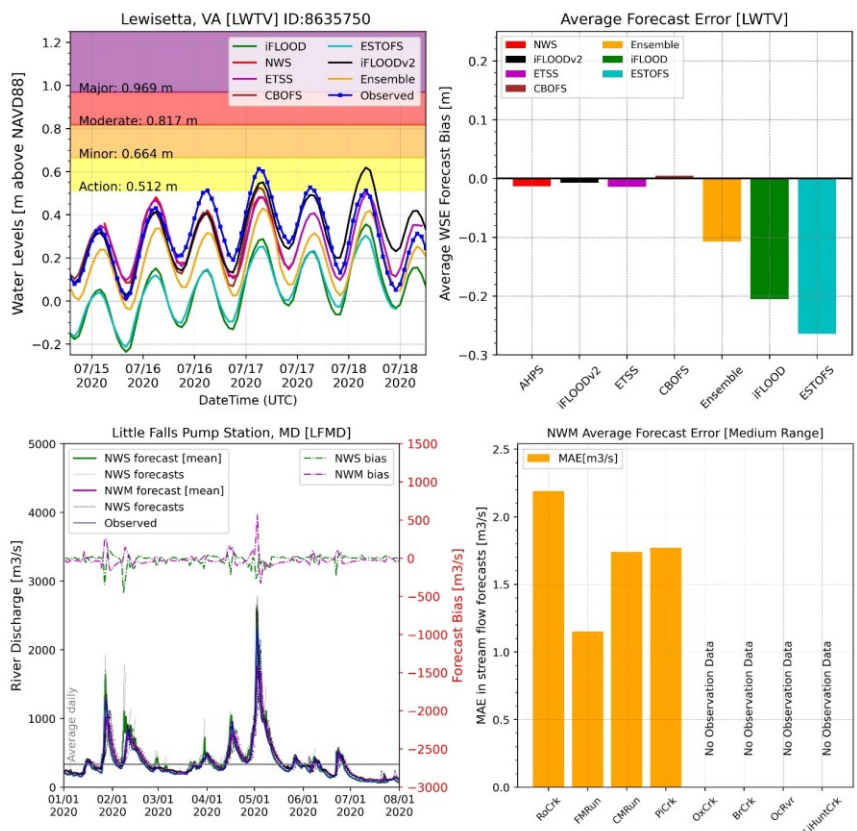


608  
 609 **Figure 8.** Maximum water levels at WASD resulting from various flood drivers.  
 610 Horizontal lines represent maximum water levels recorded at WASD during historical events.

611  
 612 **3.3. Investigation of Operational Boundary Conditions for Real-Time Total Water Level**  
 613 **Forecasting**

614  
 615 Sample forecast graphics of water levels at LWTV from all the existing coastal guidance  
 616 systems is provided in the upper left panel of **Figure 9**, while the upper right panel shows the  
 617 average forecast error (bias) at LWTV over 7 months period (Jan to Aug, 2020). Clearly, average  
 618 biases for NWS, iFLOODv2, ETSS and CBOFS are the smallest compared to all the other  
 619 guidance systems. Similarly, the forecasted stream flows of NWS and NWM for upstream major

620 rivers at LFMD is given in left lower panel of **Figure 9**, where forecast bias of NWM over 7  
 621 months period (Jan to Aug, 2020) is shown higher than NWS during observed peak stream flows.  
 622 The forecasted bias of urban runoff at the major streams over 7 months period (Jan to Aug, 2020)  
 623 in the Potomac River is also shown in Figure 9 (lower right panel), where, on average, the bias is  
 624 less than 2.5 m<sup>3</sup>/s. Forecasted wind speeds from NAM and NBM were not included in this analysis  
 625 due to lack of real-time outputs retrieved for NBM during this 8 months analysis period. This  
 626 initial assessment of forecast bias for individual guidance systems helped identify consistently high  
 627 performing guidance systems, i.e. downstream boundary (NWS, iFLOODv2, ETSS and CBOFS),  
 628 upstream major river boundary (NWS), urban runoff (NWM).



629  
 630 **Figure 9.** Sample forecast advisories and error plot (average bias and MAE) for various  
 631 forecast guidance systems a period of 8 months (Jan 2020 to Aug 2020).  
 632  
 633

634 Secondly, we performed a set of validations based on reforecast events of 2020 to demonstrate  
 635 that the above-mentioned guidance systems reduce the forecast error when modeling TWL  
 636 predictions at WASD. For the reforecast *Coastal* event, the time series of simulated total water  
 637 levels at WASD against observations (**Figure 10**, panel a) shows that the downstream boundary  
 638 provided by the NWS predicted water levels more accurately when compared to other guidance  
 639 systems (iFLOODv2, ETSS and CBOFS). The MAE resulting from the simulation using NWS as

640 boundary condition was smaller compared to other guidance systems (**Figure 10**, panel e). For the  
641 reforecast *River* event, simulated total water levels using NWS and NWM as upstream boundary  
642 conditions for major river flows showed almost the same pattern at WASD (underestimation)  
643 (**Figure 10**, panel b), however, MAE resulting from the simulation using NWS as upstream  
644 boundary condition was slightly lower than with the NWM (**Figure 10**, panel e). From the above  
645 *Coastal* and *River* reforecast analysis, upstream and downstream boundaries forecasted by the  
646 NWS are considered the best for the selected events, and further utilized to simulate a *Compound*  
647 event.

648 Panel c of **Figure 10**, shows the time series of simulated *Compound* event with and without  
649 urban drainage. MAE using the urban drainage was slightly smaller than “No Urban” flow  
650 boundary. For this specific event, the observed urban runoff was much smaller than the 25-year  
651 return period; therefore, we would not have expected any significant influence on the water levels.  
652 However, our analysis (section 3.1.3) showed that the addition of urban runoff can certainly help  
653 capture the increase in water levels around National Capital Region in the case of large urban  
654 events. Lastly, to find the best performing weather forecast model, we again simulated the  
655 *Compound* event (April 2020) without the local winds and in the presence of forecasted winds  
656 from NAM and NBM atmospheric models (**Figure 10**, panel d). Based on our hypothetical  
657 analysis (3.1.4) and the observed winds (8 m/s from SE) during this particular event, we would  
658 expect a small increase of 0.08 m to water levels at WASD. The simulated TWL using NAM  
659 weather forcing showed the expected increase (~0.1 m) based on local wind forcing, while NBM  
660 weather forcing based simulation did not show an increase. Further analysis of the wind magnitude  
661 and direction forecasted by NAM and NBM (not shown here) revealed the under prediction at  
662 WASD by NBM, while NAM accurately forecasted the high winds during *Compound* event. The  
663 MAE in the absence of local wind forcing was nearly 0.25 m, which decreased to 0.22 m using  
664 NAM wind forcing.

665

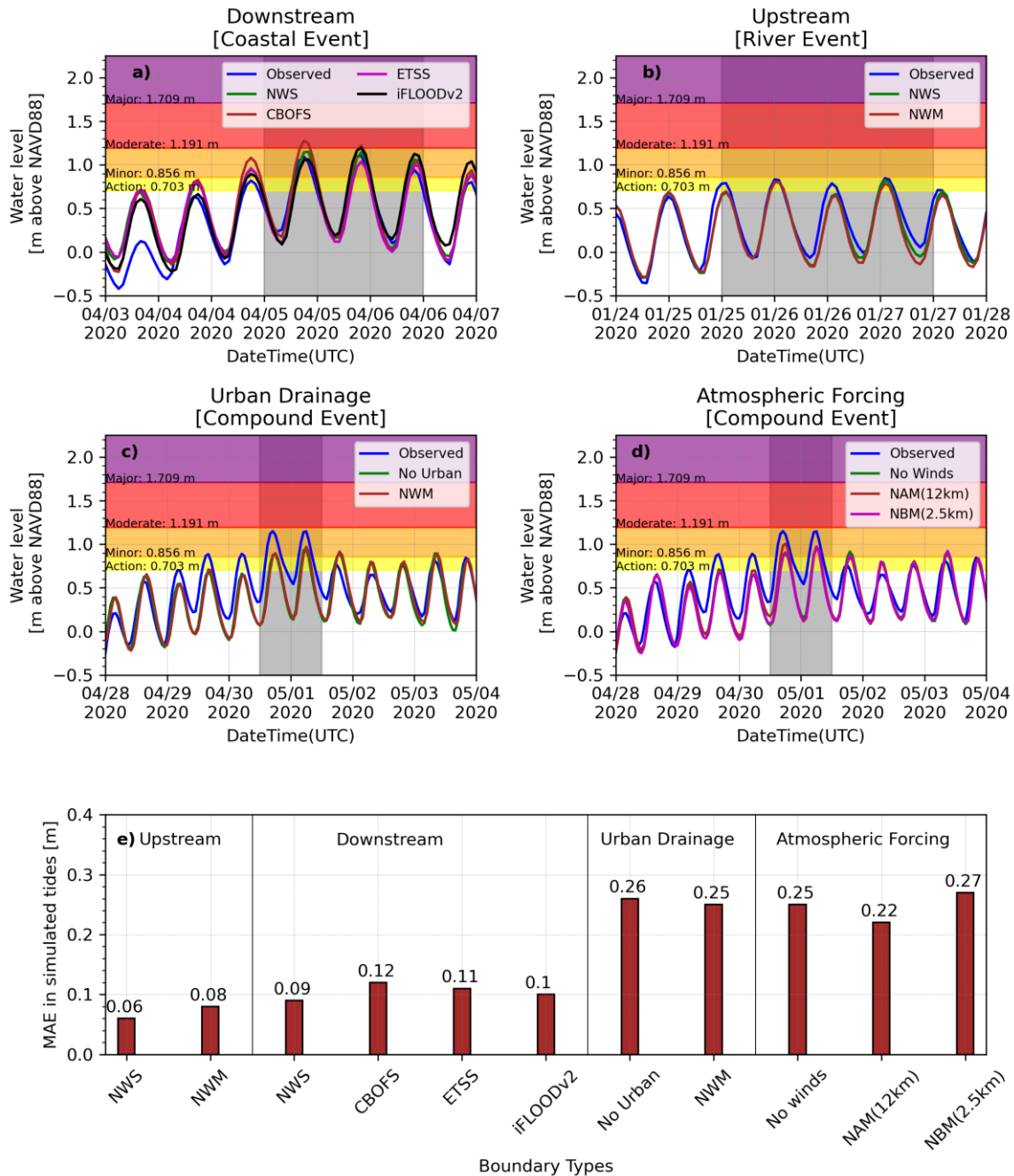


**Figure 10.** Reforecast analysis of River, Coastal and Compound events of 2020 using various boundary types at WASD station.

Although some guidance systems performed better than others for given reforecast events, a larger set of events will be required to confirm a best set of boundary guidance systems. Based on our given set of reforecast events, we proposed a recommended set of guidance systems (Table 6) for development of TWL forecast system in the Potomac River.

676

677 **Table 6.** Recommended set of boundary conditions for total water level forecasting in Potomac  
678 River based on reforecast events of 2020

<b>Boundary Types</b>	<b>Suggested Forecast/Guidance System</b>
<i>Downstream Water Levels</i>	NWS
<i>Upstream Major River Flows</i>	NWS
<i>Upstream Urban Runoff</i>	NWM
<i>Atmospheric Forcing</i>	NAM

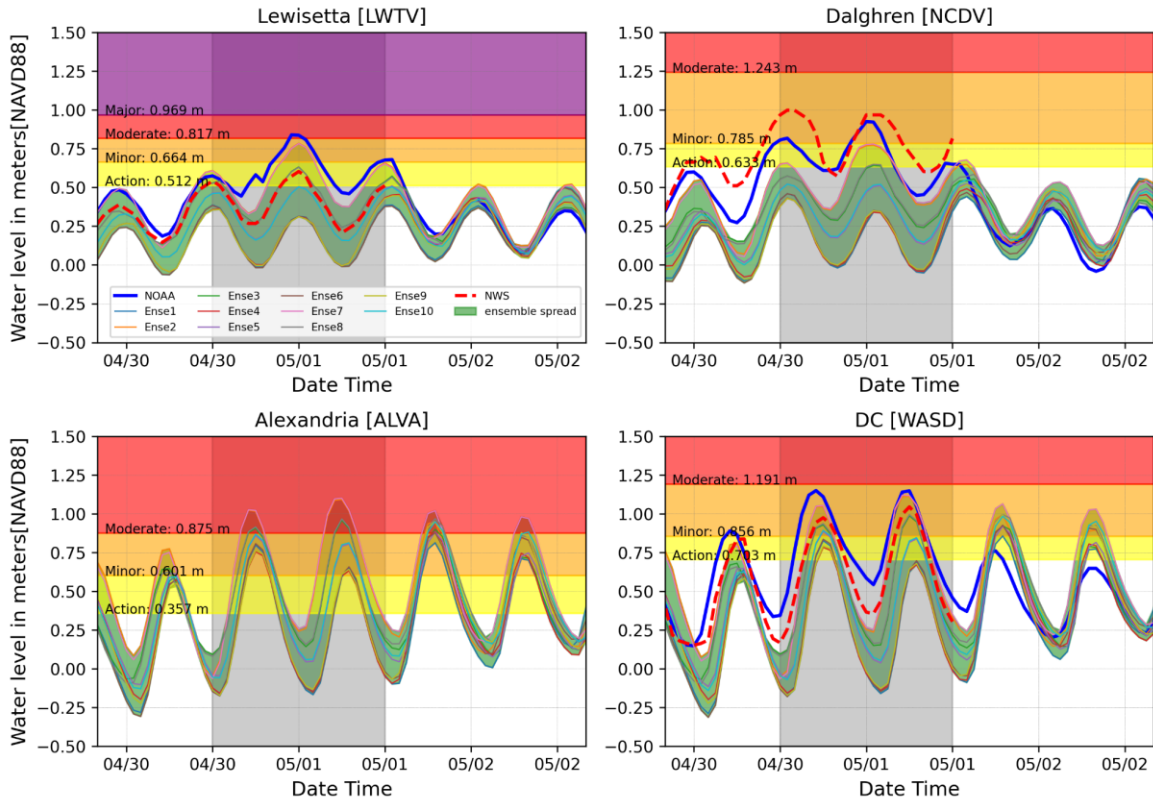
679

680

681

### 682 **3.4. Ensemble Based Forecasting**

683 The use of multi model ensembles has been shown in numerous applications (Hagedorn et  
684 al., 2005; Kirtman et al., 2014; Krishnamurti et al., 2000; Weigel et al., 2008) to improve forecast  
685 skill. Our results showed the advantage of using ensemble-based flood prediction in comparison  
686 to single value flood forecasts. Ensemble forecasts of TWL predictions during *Compound*  
687 reforecast event of 2020 using a set of 10 simulations is shown in **Figure 11**. Coastal downstream  
688 boundaries provided by CBOFS forecasted the highest water levels at LWTV, followed by NWS  
689 and then the Ensemble mean. Interestingly, significant variability in the predicted TWL, shown at  
690 LWTV was reduced as it propagated upstream at WASD. **Figure 11** shows that on 30<sup>th</sup> April 1800  
691 UTC, 6 out of 10 ensemble simulations predicted water levels at WASD exceeding the 0.856 m  
692 flood threshold, resulting in 60% chance of “Minor” flooding. Several hours later, on 1<sup>st</sup> May 0600  
693 UTC, the chance of flooding reduced to 40%, however, two ensemble simulations based on the  
694 CBOFS boundary condition, forecasted the peak TWL at WASD with high accuracy (bias less  
695 than 0.03 m).



696

697

698

699

**Figure 11.** Ensemble-based forecasting of total water levels for the *Compound* reforecast event of 2020 in Potomac River.

700

701

702

703

704

705

706

707

708

709

The upper bound of the ensemble distribution predicted total water levels at nearly all the stations with high accuracy. **Figure 11** also show that the ensemble spread grows during high flood events leading to higher forecast uncertainty and shrinks back under normal daily conditions (i.e. after 2<sup>nd</sup> May). Ensemble predictions serves as a compromise to high-resolution numerical modeling, due to its ability to capture the forecast uncertainty. This analysis showed the ability of this integrated framework to utilize ensemble-based TWL forecasting, while providing representation of uncertainty originating from selected boundary guidance systems. Although, similar to last section, one test case may not be sufficient, this briefly highlights the value of ensemble forecasting over deterministic forecasts to develop high accuracy official flood forecasts in the Upper Tidal Potomac Region using model-generated guidance.

710

#### 711 4. Conclusion

712

713

714

Real-time flood forecasting in upstream tidal areas is challenging due to the complex and dynamic interaction of several flood drivers. This study presents a detailed assessment of various flood drivers required for accurate total water level (TWL) forecasting in upstream tidal rivers.

715 The Tidal Potomac River is a representative example of a tidal river that has complex physical  
716 interaction of ocean tides, freshwater inflows, urban runoff, and local wind impacts in  
717 hydrodynamics. The existing operational coastal guidance systems frequently underestimate water  
718 levels predictions in such complex environments. This study area is of national importance, since  
719 the National Capital Region is located at the confluence of the Potomac River and the Anacostia  
720 River, and it is susceptible to an increasing threat from flooding. In this study, we utilized the  
721 ADCIRC-2DDI model to simulate these interactions and implemented a calibrated and validated  
722 model set up for the Potomac River, which was further assessed to quantify the contribution of  
723 each flood driver on the TWL at Washington, DC (WASD). Model validation results indicated  
724 that with riverine flows greater than 3000 m<sup>3</sup>/s overestimate the water levels at WASD by almost  
725 0.5 m, which was corrected before further evaluation.

726 Using a range of hypothetical boundary forcing, we have shown that the influence of  
727 downstream boundary, upstream river discharge, local urban runoff and wind forcing are important  
728 and must be considered while forecasting total water levels in the region. For instance, the  
729 downstream boundary at LWTV represents three-fourths of observed water levels at WASD,  
730 upstream major river flows as low as a 25-year return period flow can increase the water levels by  
731 almost 2.5 m above normal daily tides at WASD, and local urban runoff combined with major  
732 river flows can raise the flooding levels by almost 0.5 m (100-year return period increase equals  
733 200-year return period). Similarly, the influence of local “impact winds” (> 10 m/s) is noticeable  
734 on water levels, as it can elevate water levels ( $\pm$  0.15 to 2.25 m) above normal daily tides at WASD.  
735 Furthermore, results based on reforecast events of 2020 showed that upstream flow and  
736 downstream water level boundary forcing based on the NWS system can reasonably forecast water  
737 levels at WASD. Likewise, forecasted urban flows provided by NWM and wind forcing from  
738 NAM weather model improved the TWL estimates at WASD.

739 Although the contributions of each physical process in forecasting TWL are quantified and  
740 noted relevant, adding these boundaries in the large-scale coastal guidance systems increases the  
741 model complexity and operational computational time. Therefore, we demonstrate the value of a  
742 dedicated forecast system for complex tidal rivers of National importance, while including all these  
743 boundaries forcing (tides, storm surge, river discharge, urban runoff, and local winds) to accurately  
744 forecast the total water levels in the National Capital Region. Moreover, the additional benefit of  
745 using this dedicated system is the ability to run ensembles forecasts using a range of boundary  
746 forcing. Further evaluation of Potomac integrated system over a longer forecast period will provide  
747 a better assessment of its prediction capacity and the value added from the ensemble forecasts.

748

## 749 **5. Acknowledgements**

750 This work was made possible by Virginia Sea Grant Program [Grant # NA18OAR4170083] and  
751 the research resources from the Flood Hazards Research Lab (FHRL) at George Mason University.

752 Any opinions, findings, and conclusions or recommendations expressed in this material are those  
753 of the authors and do not necessarily reflect the views of the NWS. This work used the Extreme  
754 Science and Engineering Discovery Environment (XSEDE) STAMPEDE2 resources through  
755 allocation id TG-BCS130009, which is supported by National Science Foundation [grant number  
756 ACI- 1548562] (Towns et al., 2014). The authors acknowledge the Texas Advanced Computing  
757 Center (TACC) at The University of Texas at Austin for providing HPC resources that have  
758 contributed to the model calibration results reported within this paper  
759 (<http://www.tacc.utexas.edu>).

760

## 761 6. References

762

- 763 Atkinson, L. P., Ezer, T., & Smith, E. (2012). Sea level rise and flooding risk in Virginia. *Sea*  
764 *Grant L. & Pol'y J.*, 5, 3.
- 765 Austin, M. (2005). Creating a GIS from NOAA electronic navigational charts. In *Proceedings of*  
766 *OCEANS 2005 MTS/IEEE* (pp. 839–841).
- 767 Bacopoulos, P., Tang, Y., Wang, D., & Hagen, S. C. (2017). Integrated hydrologic-  
768 hydrodynamic modeling of estuarine-riverine flooding: 2008 Tropical Storm Fay. *Journal*  
769 *of Hydrologic Engineering*, 22(8), 4017022.
- 770 Bakhtyar, R., Maitaria, K., Velissariou, P., Trimble, B., Mashriqui, H., Moghimi, S., et al.  
771 (2020). A New 1D/2D Coupled Modeling Approach for a Riverine-Estuarine System Under  
772 Storm Events: Application to Delaware River Basin. *Journal of Geophysical Research:*  
773 *Oceans*, 125(9), e2019JC015822. <https://doi.org/10.1029/2019JC015822>
- 774 Blain, C. A., Linzell, R. S., Chu, P., & Massey, C. (2010). *Validation test report for the*  
775 *ADvanced CIRCulation Model (ADCIRC) v45. 11*. DTIC Document. Retrieved from  
776 <http://oai.dtic.mil/oai/oai?verb=getRecord&metadataPrefix=html&identifier=ADA518667>
- 777 Bobanović, J., Thompson, K. R., Desjardins, S., & Ritchie, H. (2006). Forecasting storm surges  
778 along the east coast of Canada and the North-Eastern United States: The storm of 21  
779 January 2000. *Atmosphere-Ocean*, 44(2), 151–161. <https://doi.org/10.3137/ao.440203>
- 780 Caldwell, P. C., Merrifield, M. A., & Thompson, P. R. (2015). Sea level measured by tide gauges  
781 from global oceans--the Joint Archive for Sea Level holdings (NCEI Accession 0019568),  
782 Version 5.5, NOAA National Centers for Environmental Information, Dataset. *Centers*  
783 *Environ. Information, Dataset*.
- 784 Cosgrove, B. A., Gochis, D. J., Graziano, T., Clark, E., & Flowers, T. (2018). An update on the  
785 NOAA National Water Model and related activities. In *98th American Meteorological*  
786 *Society Annual Meeting*.
- 787 Depietri, Y., Dahal, K., & McPhearson, T. (2018). Multi-hazard risks in New York City. *Natural*  
788 *Hazards and Earth System Sciences*, 18(12), 3363–3381. <https://doi.org/10.5194/nhess-18->

- 790 Dresback, K. M., Fleming, J. G., Blanton, B. O., Kaiser, C., Gourley, J. J., Tromble, E. M.,  
791 Luettich, R. A., Kolar, R. L., Hong, Y., Cooten, S. Van, et al. (2013). Skill assessment of a  
792 real-time forecast system utilizing a coupled hydrologic and coastal hydrodynamic model  
793 during Hurricane Irene (2011). <https://doi.org/10.1016/j.csr.2013.10.007>
- 794 Dresback, K. M., Fleming, J. G., Blanton, B. O., Kaiser, C., Gourley, J. J., Tromble, E. M.,  
795 Luettich, R. A., Kolar, R. L., Hong, Y., Van Cooten, S., et al. (2013). Skill assessment of a  
796 real-time forecast system utilizing a coupled hydrologic and coastal hydrodynamic model  
797 during Hurricane Irene (2011). *Continental Shelf Research*, 71, 78–94.  
798 <https://doi.org/10.1016/j.csr.2013.10.007>
- 799 Egbert, G. D., & Erofeeva, S. Y. (2002). Efficient inverse modeling of barotropic ocean tides.  
800 *Journal of Atmospheric and Oceanic Technology*, 19(2), 183–204.  
801 [https://doi.org/10.1175/1520-0426\(2002\)019<0183:EIMOBO>2.0.CO;2](https://doi.org/10.1175/1520-0426(2002)019<0183:EIMOBO>2.0.CO;2)
- 802 Funakoshi, Y., Feyen, J., Aikman, F., Tolman, H., Van Der Westhuysen, A., Chawla, A., et al.  
803 (2012). Development of extratropical surge and tide operational forecast system (ESTOFS).  
804 In *Proceedings of the International Conference on Estuarine and Coastal Modeling* (pp.  
805 201–212). <https://doi.org/10.1061/9780784412411.00012>
- 806 Funakoshi, Y., Feyen, J., Aikman, F., Tolman, H., van der Westhuysen, A., Chawla, A., et al.  
807 (2012). Development of Extratropical Surge and Tide Operational Forecast System  
808 (ESTOFS). In *Estuarine and Coastal Modeling*.  
809 <https://doi.org/10.1061/9780784412411.00012>
- 810 Garzon, J., & Ferreira, C. (2016). Storm Surge Modeling in Large Estuaries: Sensitivity  
811 Analyses to Parameters and Physical Processes in the Chesapeake Bay. *Journal of Marine*  
812 *Science and Engineering*. <https://doi.org/10.3390/jmse4030045>
- 813 Garzon, J. L., Ferreira, C. M., & Padilla-Hernandez, R. (2018). Evaluation of weather forecast  
814 systems for storm surge modeling in the Chesapeake Bay. *Ocean Dynamics*, 68(1), 91–107.  
815 <https://doi.org/10.1007/s10236-017-1120-x>
- 816 Garzon, Juan L., Ferreira, C. M., & Padilla-Hernandez, R. (2018). Evaluation of weather forecast  
817 systems for storm surge modeling in the Chesapeake Bay. *Ocean Dynamics*, 68(1), 91–107.  
818 <https://doi.org/10.1007/s10236-017-1120-x>
- 819 Gross, T. F., Bosley, K. T., & Hess, K. W. (2000). The Chesapeake Bay operational forecast  
820 system (CBOFS): technical documentation. US Department of Commerce, National  
821 Oceanic and Atmospheric Administration, National Ocean Service, Office of Coast Survey.  
822 *Coast Center for Operational Oceanographic Products and Services*.
- 823 Hagedorn, R., Doblus-Reyes, F. J., & Palmer, T. N. (2005). The rationale behind the success of  
824 multi-model ensembles in seasonal forecasting—I. Basic concept. *Tellus A: Dynamic*  
825 *Meteorology and Oceanography*, 57(3), 219–233.
- 826 Hanson, J., Wadman, H., Blanton, B., & Roberts, H. (2013). *ERDC/CHL TR-11-1 “Coastal*

- 827 *Storm Surge Analysis: Modeling System Validation; Report 4: Intermediate Submission No.*  
828 *2.0.* Retrieved from [www.erdc.usace.army.mil](http://www.erdc.usace.army.mil).
- 829 Herdman, L., Erikson, L., & Barnard, P. (2018). Storm surge propagation and flooding in small  
830 tidal rivers during events of mixed coastal and fluvial influence. *Journal of Marine Science*  
831 *and Engineering*, 6(4), 158.
- 832 Ikeuchi, H., Hirabayashi, Y., Yamazaki, D., Muis, S., Ward, P. J., Winsemius, H. C., et al.  
833 (2017). Compound simulation of fluvial floods and storm surges in a global coupled river-  
834 coast flood model: Model development and its application to 2007 Cyclone Sidr in  
835 Bangladesh. *Journal of Advances in Modeling Earth Systems*, 9(4), 1847–1862.  
836 <https://doi.org/10.1002/2017MS000943>
- 837 Jongman, B., Ward, P. J., & Aerts, J. C. J. H. (2012). Global exposure to river and coastal  
838 flooding: Long term trends and changes. *Global Environmental Change*, 22(4), 823–835.  
839 <https://doi.org/10.1016/j.gloenvcha.2012.07.004>
- 840 Kerr, P. C., Donahue, A. S., Westerink, J. J., Luettich, R. A., Zheng, L. Y., Weisberg, R. H., et  
841 al. (2013). U.S. IOOS coastal and ocean modeling testbed: Inter-model evaluation of tides,  
842 waves, and hurricane surge in the Gulf of Mexico. *Journal of Geophysical Research:*  
843 *Oceans*, 118(10), 5129–5172. <https://doi.org/10.1002/jgrc.20376>
- 844 Khalid, A., & Ferreira, C. (2020). Advancing real-time flood prediction in large estuaries:  
845 iFLOOD a fully coupled surge-wave automated web-based guidance system. *Environmental*  
846 *Modelling & Software*, 104748. <https://doi.org/10.1016/j.envsoft.2020.104748>
- 847 Kim, S.-C., Chen, J., & Shaffer, W. A. (1996). An operational forecast model for extratropical  
848 storm surges along the US east coast. In *Preprints Conference on Coastal Oceanic and*  
849 *Atmospheric Prediction, Atlanta, Amer. Meteor. Soc* (pp. 281–286).
- 850 Kirtman, B. P., Min, D., Infanti, J. M., Kinter III, J. L., Paolino, D. A., Zhang, Q., et al. (2014).  
851 The North American multimodel ensemble: phase-1 seasonal-to-interannual prediction;  
852 phase-2 toward developing intraseasonal prediction. *Bulletin of the American*  
853 *Meteorological Society*, 95(4), 585–601.
- 854 Kourafalou, V. H., De Mey, P., Le Hénaff, M., Charria, G., Edwards, C. A., He, R., et al. (2015).  
855 Coastal Ocean Forecasting: system integration and evaluation. *Journal of Operational*  
856 *Oceanography*, 8(sup1), s127–s146. <https://doi.org/10.1080/1755876X.2015.1022336>
- 857 Krishnamurti, T. N., Kishtawal, C. M., Zhang, Z., LaRow, T., Bachiochi, D., Williford, E., et al.  
858 (2000). Multimodel ensemble forecasts for weather and seasonal climate. *Journal of*  
859 *Climate*, 13(23), 4196–4216.
- 860 Loftis, D., & Forrest, D. (2018). Citizen-Science’s Role in Flooding Resiliency: Tracing Today’s  
861 King Tides to Validate a Street-Level Hydrodynamic Model and Responsibly Reduce Risk  
862 for the Floods of Tomorrow. *AGUFM, 2018, NH23B--06*.
- 863 Luettich, R. A., Westerink, J. J., & Scheffner, N. (1992). *ADCIRC: an advanced three-*  
864 *dimensional circulation model for shelves coasts and estuaries, report 1: theory and*

865 *methodology of ADCIRC-2DDI and ADCIRC-3DL. Dredging Research Program Technical*  
866 *Report DRP-92-6, U.S. Army Engineers Waterways Experiment Station, Vicksburg, MS.*

867 Lyddon, C., Brown, J. M., Leonardi, N., & Plater, A. J. (2018). Uncertainty in estuarine extreme  
868 water level predictions due to surge-tide interaction. *PLOS ONE*, *13*(10), 1–17.  
869 <https://doi.org/10.1371/journal.pone.0206200>

870 Mashriqui, H. S., Halgren, J. S., & Reed, S. M. (2014). A 1D River Hydraulic Model for  
871 Operational Flood Forecasting in the Tidal Potomac: Evaluation for Freshwater, Tidal, and  
872 Wind Driven Events 4 5 6. Retrieved from  
873 <http://www.nws.noaa.gov/oh/hrl/modelcalibration/6>. Hydraulic Model  
874 Calibration/potomac\_modeling\_JHE.pdf

875 McDowell, M. (2016). *Comparison of Hydrologic and Hydraulic Characteristics of the*  
876 *Anacostia River to Non-Urban Coastal Streams.*

877 Mied, R. P., Donato, T. F., & Friedrichs, C. T. (2006). Eddy generation in the tidal Potomac  
878 River. *Estuaries and Coasts*, *29*(6), 1067–1080. <https://doi.org/10.1007/BF02781810>

879 Möller, O. O., Castaing, P., Salomon, J.-C., & Lazure, P. (2001). The influence of local and non-  
880 local forcing effects on the subtidal circulation of Patos Lagoon. *Estuaries*, *24*(2), 297–311.  
881 <https://doi.org/10.2307/1352953>

882 Ray, T., Stepinski, E., Sebastian, A., & Bedient, P. B. (2011). Dynamic Modeling of Storm  
883 Surge and Inland Flooding in a Texas Coastal Floodplain. *Journal of Hydraulic*  
884 *Engineering*, *137*(10), 1103–1110. [https://doi.org/10.1061/\(asce\)hy.1943-7900.0000398](https://doi.org/10.1061/(asce)hy.1943-7900.0000398)

885 Ries III, K. G., Newson, J. K., Smith, M. J., Guthrie, J. D., Steeves, P. A., Haluska, T. L., et al.  
886 (2017). *StreamStats, version 4.*

887 Roberts, K. J., Pringle, W. J., & Westerink, J. J. (2019). OceanMesh2D 1.0: MATLAB-based  
888 software for two-dimensional unstructured mesh generation in coastal ocean modeling.  
889 *Geoscientific Model Development*, *12*(5), 1847–1868. [https://doi.org/10.5194/gmd-12-1847-](https://doi.org/10.5194/gmd-12-1847-2019)  
890 [2019](https://doi.org/10.5194/gmd-12-1847-2019)

891 Santiago-Collazo, F. L., Bilskie, M. V., & Hagen, S. C. (2019). A comprehensive review of  
892 compound inundation models in low-gradient coastal watersheds. *Environmental Modelling*  
893 *and Software*, *119*(June), 166–181. <https://doi.org/10.1016/j.envsoft.2019.06.002>

894 Shen, J., Wang, H., Sisson, M., & Gong, W. (2006). Storm tide simulation in the Chesapeake  
895 Bay using an unstructured grid model. *Estuarine, Coastal and Shelf Science*, *68*(1), 1–16.  
896 <https://doi.org/10.1016/j.ecss.2005.12.018>

897 Sumi, S. J., & Ferreira, C. (2019). Compound Urban Flooding in Large Metropolitan Areas  
898 along Tidal Rivers: A Case Study for the Washington DC Region. *AGUFM, 2019*, H13J--  
899 1821.

900 Svensson, C., & Jones, D. A. (2004). Dependence between sea surge, river flow and precipitation  
901 in south and west Britain. *Hydrology and Earth System Sciences*, *8*(5), 973–992.  
902 <https://doi.org/10.5194/hess-8-973-2004>

903 Thatcher, C. A., Brock, J. C., Danielson, J. J., Poppenga, S. K., Gesch, D. B., Palaseanu-  
904 Lovejoy, M. E., et al. (2016). Creating a Coastal National Elevation Database (CoNED) for  
905 science and conservation applications. *Journal of Coastal Research*, (76), 64–74.

906 Towns, J., Cockerill, T., Dahan, M., Foster, I., Gaither, K., Grimshaw, A., et al. (2014). XSEDE:  
907 Accelerating scientific discovery. *Computing in Science and Engineering*, 16(5), 62–74.  
908 <https://doi.org/10.1109/MCSE.2014.80>

909 Tshimanga, R. M., Tshitenge, J. M., Kabuya, P., Alsdorf, D., Mahe, G., Kibukusa, G., &  
910 Lukanda, V. (2016). A Regional Perceptive of Flood Forecasting and Disaster Management  
911 Systems for the Congo River Basin. In *Flood Forecasting* (pp. 87–124). Elsevier.

912 Wahl, T., Jain, S., Bender, J., Meyers, S. D., & Luther, M. E. (2015). Increasing risk of  
913 compound flooding from storm surge and rainfall for major US cities. *Nature Climate*  
914 *Change*, 5(12), 1093–1097. <https://doi.org/10.1038/nclimate2736>

915 Walsh, C. J., Fletcher, T. D., & Burns, M. J. (2012). Urban Stormwater Runoff: A New Class of  
916 Environmental Flow Problem. *PLOS ONE*, 7(9), 1–10.  
917 <https://doi.org/10.1371/journal.pone.0045814>

918 Wang, H. V, Loftis, J. D., Forrest, D., Smith, W., & Stamey, B. (2015). Modeling Storm Surge  
919 and Inundation in Washington, DC, during Hurricane Isabel and the 1936 Potomac River  
920 Great Flood. *Journal of Marine Science and Engineering*, 3(3), 607–629.  
921 <https://doi.org/10.3390/jmse3030607>

922 Weigel, A. P., Liniger, M. A., & Appenzeller, C. (2008). Can multi-model combination really  
923 enhance the prediction skill of probabilistic ensemble forecasts? *Quarterly Journal of the*  
924 *Royal Meteorological Society: A Journal of the Atmospheric Sciences, Applied Meteorology*  
925 *and Physical Oceanography*, 134(630), 241–260.

926 Wessel, P., & Smith, W. H. F. (1996). A global, self-consistent, hierarchical, high-resolution  
927 shoreline database. *Journal of Geophysical Research: Solid Earth*, 101(B4), 8741–8743.  
928 <https://doi.org/10.1029/96jb00104>

929 Wu, W., McInnes, K., O’Grady, J., Hoeke, R., Leonard, M., & Westra, S. (2018). Mapping  
930 Dependence Between Extreme Rainfall and Storm Surge. *Journal of Geophysical Research:*  
931 *Oceans*, 123(4), 2461–2474. <https://doi.org/10.1002/2017JC013472>

932 Zheng, F., Westra, S., & Sisson, S. A. (2013). Quantifying the dependence between extreme  
933 rainfall and storm surge in the coastal zone. *Journal of Hydrology*, 505, 172–187.  
934 <https://doi.org/10.1016/j.jhydrol.2013.09.054>

935 Zhong, L., Li, M., & Foreman, M. G. G. (2008). Resonance and sea level variability in  
936 Chesapeake Bay. *Continental Shelf Research*, 28(18), 2565–2573.

937

938

939 **7. Appendix**

940

941

942

943

**Table A1.** List of Stations in the Study area

<b>Region</b>	<b>Station Full Name</b>	<b>Abbreviation</b>	<b>Long</b>	<b>Lat</b>	<b>Observed Water</b>	<b>Observed Flow</b>	<b>Tide Prediction</b>
<i>Potomac Upper River Reach</i>	Little Falls Pump Station, MD	LFMD	-77.13	38.95	Y	Y	-
	Wisconsin Ave, DC	WADC	-77.07	38.90	Y	-	-
<i>Anacostia River Reach</i>	Northeast Branch Riverdale, MD	NEMD	-76.93	38.96	-	Y	-
	Northwest Branch Hyattsville, MD	NWMD	-76.97	38.95	-	Y	-
	Bladensburg, MD	BDMD	-76.94	38.93	-	-	Y
	East Lake, MD	ELMD	-76.96	38.91	-	-	Y
	Kingman Lake, MD	KLMD	-76.97	38.89	-	-	Y
	Washington Navy Yard, DC	WNDC	-76.99	38.87	-	-	Y
	Washington, DC	WASD	-77.02	38.87	-	-	Y
	Bellevue, DC	BEDC	-77.03	38.83	-	-	Y
	Alexandria, VA	ALVA	-77.04	38.80	-	-	Y
	Fourmile Run, VA	FMVA	77.05	38.84	Y	-	-
<i>Main Potomac River</i>	Fourmile Run, Stream Station, VA	FSVA	77.09	38.84	-	Y	-
	Cameron St Dock at Alexandria, VA	CSVA	77.04	38.81	Y	-	-
	Cameron Run at Alexandria, VA	CRVA	77.11	38.80	-	Y	-
	Piscataway Creek, MD	PCMD	76.97	38.71	-	Y	-
	Marshall Hall, MD	MHMD	-77.10	38.69	-	-	Y
	Indian Head, MD	IHMD	-77.19	38.60	-	-	Y
	Quantico, VA	QUVA	-77.29	38.52	-	-	Y
	Liverpool Point, MD	LPMD	-77.27	38.46	-	-	Y
	Clifton Beach, Smith Point, MD	CLMD	-77.27	38.41	-	-	Y
	Riverside, MD	RSMD	-77.14	38.39	-	-	Y
	Goose Creek, MD	GCMD	-77.05	38.45	-	-	Y
	Mathias Point, VA	MPVA	-77.06	38.40	-	-	Y
	Dalghren, VA	NCDV	-77.04	38.32	Y	-	Y
	Lower Cedar Point, MD	LCMD	-76.98	38.34	-	-	Y
	Colonial Beach, Potomac River, VA	COVA	-76.96	38.25	-	-	Y
Colton Point, MD	CPMD	-76.75	38.22	-	-	Y	
Ragged Point, VA	RPVA	-76.61	38.14	-	-	Y	
Piney Point, MD	PPMD	-76.53	38.13	-	-	Y	
Lewisetta, VA	LWTV	-76.47	37.99	Y	-	Y	

944

945

946

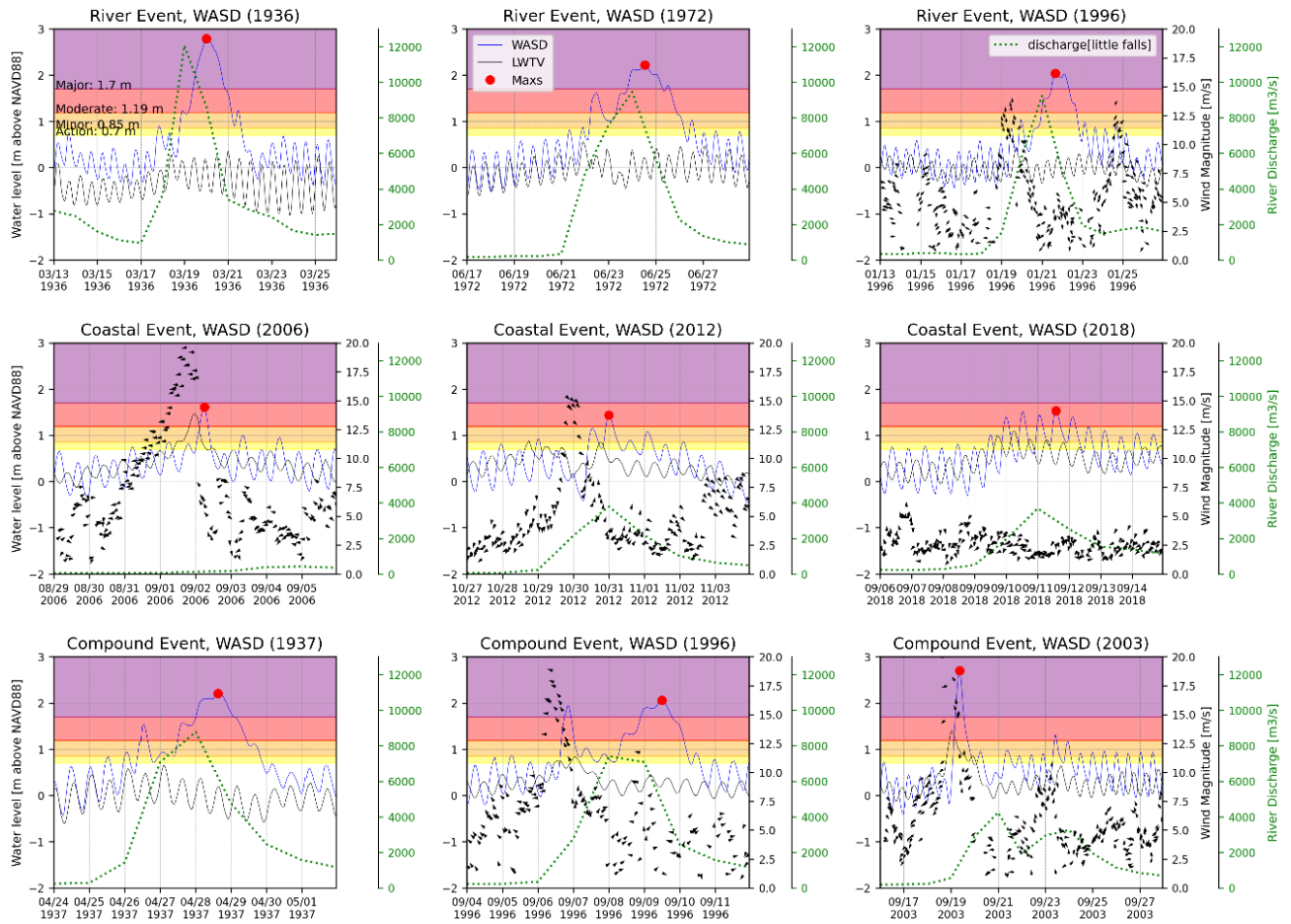
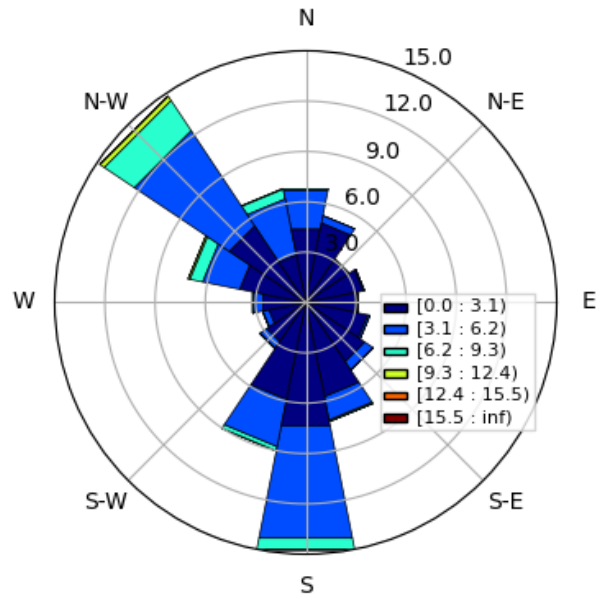


Figure A1. Time series of observed data for various case studies

948  
949  
950  
951  
952  
953  
954

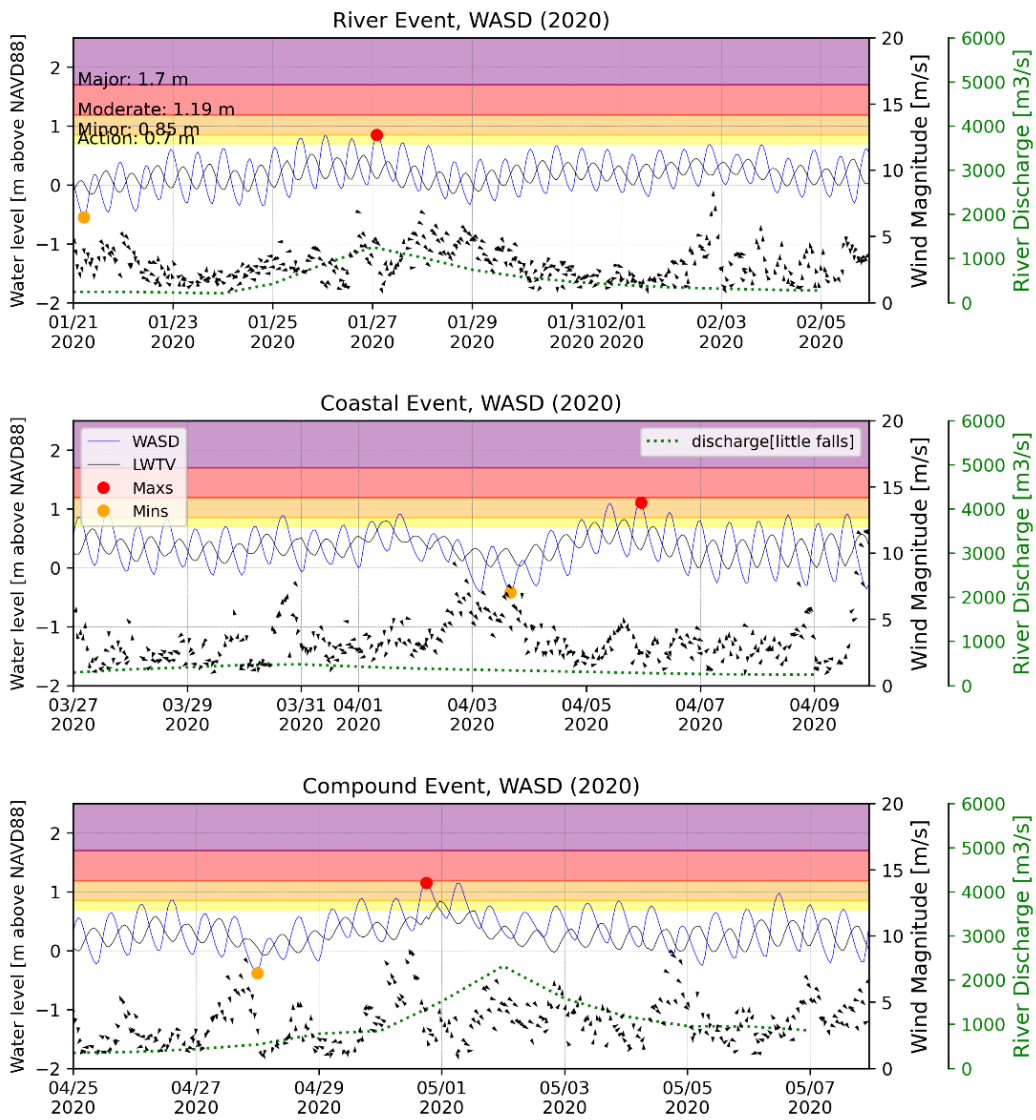


955

956

**Figure A2.** Wind rose plot for the observed winds at WASD from 2008 to 2020

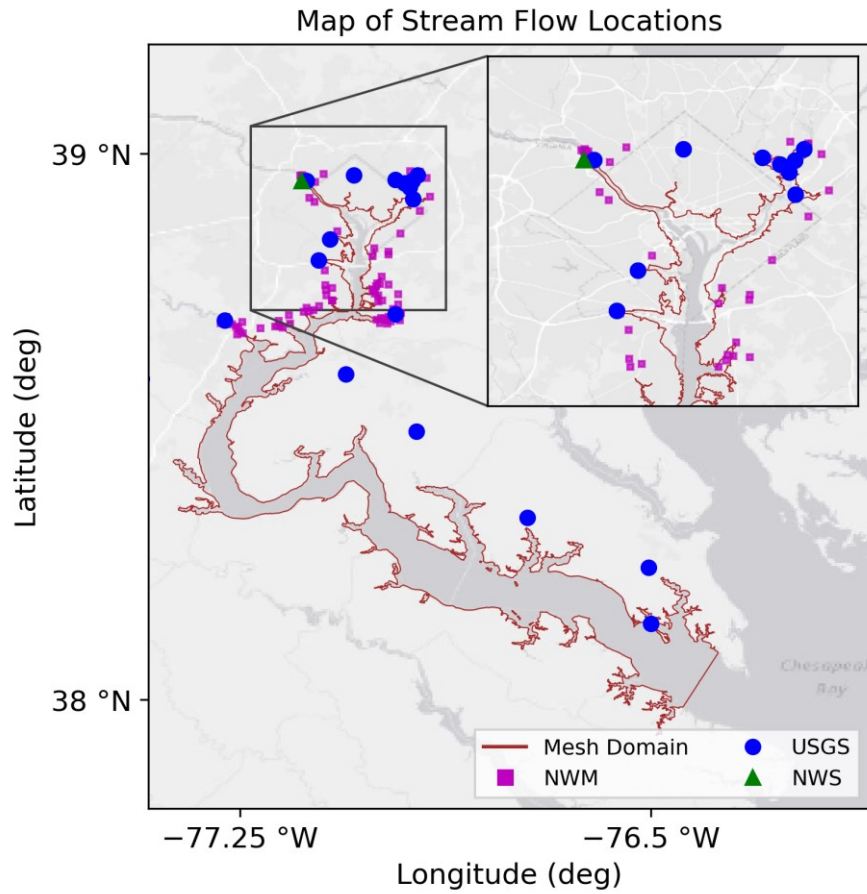
957



958

959

**Figure A3.** Time series of observed data for various case studies



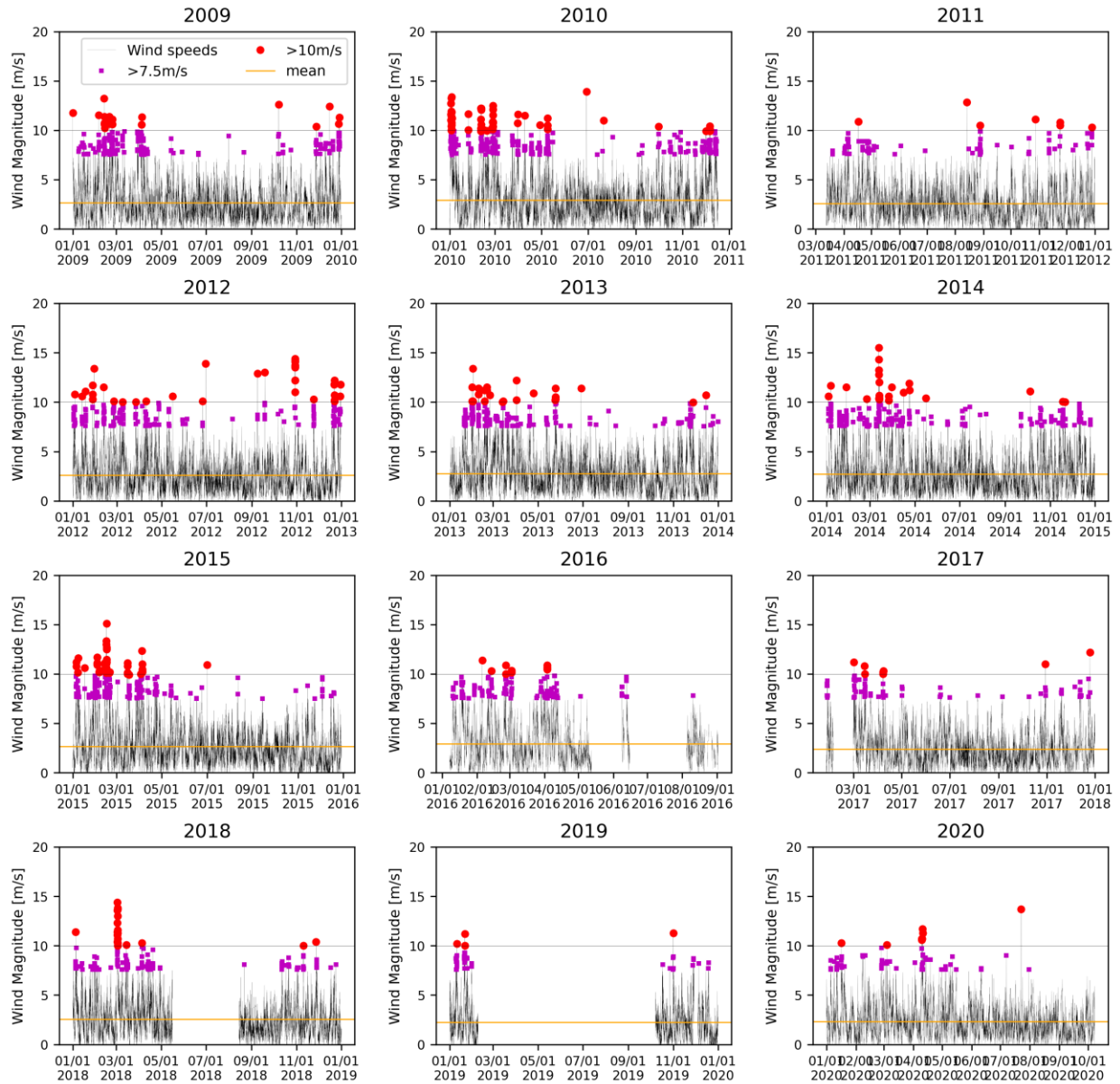
960

961

**Figure A4.** Location map of USGS, NWS and NWM observation and forecast stations.

962

963



964

965

966 **Figure A5.** Observed wind speeds (above 10m height) at WASD during the period of 12  
 967 consecutive years (2009 to 2020)

968

969

## 970 **Data Availability Statement**

971 All model analyses in this study were conducted on behalf of the Mason Flood Hazards Research Lab  
972 (<https://fhrl.vse.gmu.edu/>) and are stored on the local servers. The modeling outputs are available for non-  
973 commercial, academic research purposes, only upon reasonable request from the corresponding author.  
974 Hydrodynamic coastal storm surge model, ADCIRC, is available for non-commercial, academic research  
975 purposes, by contacting Crystal Fulcher at the University of North Carolina ([cfulcher@email.unc.edu](mailto:cfulcher@email.unc.edu)). The  
976 integrated modeling framework used in this research was based on the recently published iFLOOD paper  
977 (<https://doi.org/10.1016/j.envsoft.2020.104748>) and is available to view on the iFLOOD web portal  
978 (<https://iflood.vse.gmu.edu/map>). Historical observational data for winds and water level was retrieved from  
979 NOAA tides and currents database (<https://api.tidesandcurrents.noaa.gov/api/prod/>) while the streamflow data  
980 was available online at USGS water database (<https://waterdata.usgs.gov/nwis>). The streamflow data at a given  
981 return period was calculated using the online StreamStats server available at <https://streamstats.usgs.gov/ss/>.  
982 The real-time input forcing of streamflow (NWM), water level guidance (ESTOFS, ETSS) and winds (NAM,  
983 NBM) for upstream and downstream boundaries were downloaded daily from the NOAA NOMADs server  
984 available at <https://nomads.ncep.noaa.gov/pub/data/nccf/com/>. The water level forecasts from CBOFS model  
985 were available at <http://opendap.co-ops.nos.noaa.gov/netcdf/>. The iFLOODv2 forecasts were also downloaded  
986 daily from the iFLOOD online data repository available at  
987 [https://data.iflood.vse.gmu.edu/?prefix=Forecast/ChesapeakeBay\\_ADCIRCSWAN/](https://data.iflood.vse.gmu.edu/?prefix=Forecast/ChesapeakeBay_ADCIRCSWAN/)  
988 The NWS forecasts of water level and stream flows were downloaded on daily basis and are available at  
989 <https://water.weather.gov/ahps2/forecasts.php?wfo=lwx>.  
990